CNWRA *A center of excellence in earth sciences and engineering*

A Division of Southwest Research Institute
6220 Culebra Road • San Antonio, Texas, U.S.A. 78228-5166
(210) 522-5160 • Fax (210) 522-5155

April 26, 2000
Contract No. NRC-02-97-009
Account No. 20.01402.661

U.S. Nuclear Regulatory Commission
ATTN: Mr. Jeffrey Pohle
Division of Waste Management
TWFN, Mail Stop 7-D13
11545 Rockville Pike
Washington, DC 20555

Subject: Thermal Effects on Flow KTI Intermediate Milestone No. 01402.661.010: Mountain-Scale Thermal-Hydrologic Analyses—Status Report

Dear Mr. Pohle:

Enclosed please find the paper titled "Geomechanical and Thermal Effects on Moisture Flow at the Proposed Yucca Mountain Nuclear Waste Repository." In accordance to my verbal agreement with you, this deliverable is being submitted to you as a journal paper instead of a status report that was originally identified in the Operations Plan. This technical document fulfills the requirements for the subject milestone, which is due April 30, 2000.

This paper presents results of numerical-model calculations performed to estimate the effects of discrete geologic features and thermal-mechanical (TM) altered zones on the distributions of percolation flux and thermally driven moisture at the proposed repository horizon at Yucca Mountain. Thermal-hydrologic flow was simulated using a site-scale model. The geometrical and hydrological characteristics of TM altered zones were developed through separate TM modeling. The results indicate that models used to estimate the occurrence and magnitudes of water influx into emplacement drifts and the variations of relative humidity within the drifts need to consider (a) the location of the drifts relative to faults that intersect the Paintbrush Nonwelded Unit and (b) the development, geometry, and hydrological characteristics of TM altered zones. These results provide technical bases for two TEF KTI and one RDTME KTI subissues, which are identified in the paper.

If you have any questions on this report, please contact me at (210) 522-5151 or Goodluck Ofoegbu at (210) 522-6641.

Sincerely yours,

Asadul H. Chowdhury, Manager
Mining, Geotechnical, and
Facility Engineering

AHC/cap
Enclosure

Geomechanical and Thermal Effects on Moisture Flow at the Proposed Yucca Mountain Nuclear Waste Repository[1]

Goodluck I. Ofoegbu[2], Scott Painter, Rui Chen, Randall W. Fedors, and David A. Ferrill

Center for Nuclear Waste Regulatory Analyses

Southwest Research Institute

6220 Culebra Road

San Antonio Texas 78238-5166

[1]Submitted for publication in *Nuclear Technology*: April 2000

[2]Phone: (210) 522-6641, Fax: (210) 522-6081, e-mail: gofoegbu@swri.org

ABSTRACT

The percolation flux through the unsaturated zone at the proposed Yucca Mountain repository for high-level nuclear waste can potentially affect (a) the occurrence and magnitude of water influx into the emplacement drifts, (b) the onset and rates of waste-package corrosion, (c) the mobilization of waste into aqueous states, and (d) the transport of radionuclides to the saturated zone. The magnitude and spatial and temporal variations of percolation flux depend on the infiltration rate but may be significantly influenced by (a) lateral diversion of flow at stratigraphic interfaces between nonwelded and welded tuffs above the repository horizon, (b) focusing of flow within or near steeply dipping fault zones, and (c) lateral diversion of flow within thermal-mechanical altered zones. Results from numerical modeling are presented to argue that (a) areas of the repository located close to and on the up-dip side of faults that intersect the PTn would experience elevated percolation flux, irrespective of whether the faults act as flow barriers or conduits; (b) mechanical response of the rock mass to waste-generated heat will likely cause the development of laterally discontinuous zones characterized by dilation of horizontal fractures and net dilation or closure of vertical fractures; (c) areas of the repository located on the downstream side of the thermal-mechanical altered zones would experience elevated percolation flux; and (d) repository areas subjected to elevated percolation flux would experience faster rewetting of dryout zones and, thus, longer periods of wetness and elevated humidity. These results indicate that models used to predict the occurrence and magnitudes of water influx into emplacement drifts and the variations of relative humidity within the drifts need to consider the location of the drifts relative to faults that intersect the PTn and the development, geometry, and hydrological characteristics of thermal-mechanical altered zones.

INTRODUCTION

The U.S. Department of Energy has proposed a geologic repository for high-level nuclear waste at Yucca Mountain, a semiarid desert mountain in southern Nevada. The proposed site lies within a sequence of welded and nonwelded and variably fractured volcanic tuffs.[1] The repository is located in the unsaturated zone, approximately at 300 m above the water table and about the same distance below the ground surface. The waste would be encased in cylindrical metal containers (waste packages) and placed in a horizontal array of underground openings (emplacement drifts). One design option being considered relies on the emplacement drifts remaining dry for long periods of time to slow down the corrosion of the waste packages and, consequently, delay the release of radionuclides to the environment. Heat produced by radioactive decay of nuclear waste would vaporize and drive away moisture from the vicinity of the emplacement drifts and prevent moisture return to the resulting dry zones for a long time.

The extent and longevity of such dry zones depend on the thermal load (i.e., the heat output and spatial distribution of the waste packages) and the amount of water seepage (percolation flux) through the repository horizon. For a given thermal load, the percolation flux determines whether such dry zones may develop, how fast they develop, and how long they remain dry. Areas of the repository that receive higher percolation flux will be less likely to experience drying of the emplacement drifts, and the dry zones that develop in such areas will rewet faster than dry zones in areas of lower percolation flux. In addition to its effect on the drying and rewetting of the emplacement drifts, the percolation flux also determines how fast and in what quantities radionuclides may be transported down to the saturated zone after containment failure.

As a result, an understanding of the magnitudes and distributions of percolation flux and how they may be affected by the waste-generated heat is essential to predicting the

occurrence and magnitudes of seepage into the emplacement drifts, the onset and rates of waste-package corrosion, and the transport of radionuclides in aqueous states to the saturated zone. The percolation flux at the repository horizon depends on the net infiltration rate from the ground surface and the hydrological characteristics of the overlying rock units. The time-averaged infiltration rate at Yucca Mountain varies spatially from less than 1 mm/yr to about 40 mm/yr, depending on factors such as soil and vegetation cover and topographic relief.[1, 2, 3, 4, 5] The spatial average of the time-averaged infiltration rate lies in the range of 5–15 mm/yr. The hydrological characteristics of the rock units are controlled by the degrees of welding and fracturing. Generally, the welded units have low matrix porosity and permeability but are highly fractured; the nonwelded units have higher matrix porosity and permeability but lower fracture density. Consequently, water flow in the unsaturated zone is fracture dominated in the welded units whereas matrix flow is an important contributor to the overall water flux through the nonwelded units. This contrast between significant matrix flow in the nonwelded units and fracture-dominated flow in the welded units results in a capillary barrier at the contacts between the nonwelded and welded rock units.

As a result, a fraction of the vertical percolation flux entering a nonwelded unit that is underlain by a welded unit may be diverted into lateral flux. Similarly, flux diversion from lateral to vertical may occur as a result of a change in property or lateral continuity of the nonwelded rock unit. For example, results from an earlier numerical-model study[6] indicate the occurrence of a significant lateral flux in a nonwelded unit above the repository horizon and increased vertical flux on the up-dip side of a fault where the nonwelded unit is juxtaposed against a welded unit on the down-dip side. Consequently, the characteristics of the nonwelded rock units above the repository horizon that may affect the repository-level percolation flux include (a) the structural attitude of the rock unit, which has a strong effect on the occurrence and direction of lateral flow; (b) lateral change in properties (such as porosity, permeability, and capillarity), which may cause an interruption of lateral flow; and

(c) a change in the lateral continuity of the unit, such as may result from faulting.

Characteristics of the welded rock units that may affect the percolation flux are the aperture, continuity, and frequency of fractures. Because the proposed repository horizon lies within welded rock units, there is concern that the fracture attributes important to flow may be altered significantly by thermally driven geomechanical and geochemical processes during the period of regulatory concern.[7] All three fracture attributes important to flow may change as a result of thermally driven mechanical deformation (in addition to deformations induced by excavation and potential seismic loading). If mechanical deformation consists mainly of movement on preexisting fractures, as would be expected for an already fractured rock mass, then changes in fracture aperture would be more likely than changes in fracture frequency or continuity. Consequently, the welded and densely fractured rock units within the influence zone of heat generated from radioactive decay of the emplaced nuclear waste can be expected to experience fracture-aperture changes caused by thermally driven mechanical deformation.

The current study examines potential geomechanical effects on the distributions of percolation flux at the repository horizon and how the percolation flux may interact with thermally driven moisture. The geomechanical effects considered are (a) preexisting geomechanical effects, which are manifested through structural-geologic features such as faults and the associated effects on hydrological properties and (b) anticipated future geomechanical effects associated with the mechanical response of the rock mass to heat generated from radioactive decay of nuclear waste. A series of numerical analyses was conducted using a site-scale thermal-hydrological model in which the hydrological properties were selectively modified to represent zones that have been altered by faulting or are anticipated to be altered by thermal-mechanical effects. The anticipated fracture-aperture changes from thermally induced geomechanical effects and the geometrical characteristics of the zones within which such changes occur were determined from thermal-mechanical modeling.

The analysis results indicate that the vertical percolation flux at the repository horizon may vary significantly within the proposed waste-emplacement area, because of the structural-geologic features in the overlying nonwelded rock units and the anticipated thermally induced fracture-aperture changes within and close to the emplacement area. Relatively high percolation flux can be expected on the up-dip side of faults that intersect the overlying nonwelded Paintbrush Tuff unit. Also, areas of elevated flux and adjoining areas of reduced flux can be expected to occur within zones that experience thermally induced fracture-aperture changes. It is argued that these observations provide additional support for two of the key technical issues that are considered by the Nuclear Regulatory Commission to be critical to the long-term performance of the proposed Yucca Mountain repository.[8]

Study Area

The study domain is an east-west vertical section through Yucca Mountain that extends from E 169,926 to E 172,212 m along N 232,715 m (in Nevada State Plane coordinates). The section line passes through the intersection of the Solitario Canyon Fault and a north-northeast–south-southwest trending fault splay in the west and Antler Ridge in the east,[9, 10] at about the middle of the southern half of the proposed repository block.[11] The stratigraphy of the model section (Fig. 1) was extracted from a three-dimensional geologic framework model of Yucca Mountain.[12] The hydrogeological units encountered in the section are (in top-down order) the Tiva Canyon welded tuff (TCw), Paintbrush nonwelded tuff (PTn), Topopah Spring welded tuff (TSw), and the Calico Hills nonwelded tuff (CHn). The hydrogeological units have been subdivided into smaller subunits (model layers) by the Yucca Mountain Project (YMP)[13, 14] to better represent the vertical variation of hydrological properties (Table I). The PTn was, however, treated as a single unit in the current model despite its division into five subunits in the YMP model, for reasons of computational expediency.

Geologic Features Important to Flow

Yucca Mountain consists of a thick accumulation of gently east-dipping Miocene volcanic tuff layers that are cut by an array of primarily north-trending normal faults and northwest-trending dextral strike-slip faults.[9, 10] The larger faults in the two dominant orientations bound major fault blocks at Yucca Mountain. The two sets of faults are interpreted to be coeval, based on mutual terminations and secondary structures between them such as pull-apart basins.[9] Some northwest-trending faults are dominantly normal faults, accommodating extension in relay ramps between overlapping normal faults.[10, 15, 16] Four reverse faults with north-south or northeast-southwest strikes have also been identified at Yucca Mountain.[9, 10] In addition to block bounding faults, there are numerous intrablock faults at Yucca Mountain, which include fault splays, relict fault tips,[16] connecting faults,[15] and isolated intrablock faults.[10]

The proposed repository area is bounded on the west by the Solitario Canyon Fault, and some of its splay faults, and on the east by the Ghost Dance Fault (GDF), a major intrablock fault.[9, 10] Major intrablock faults that cut through the repository block include the north end of the Abandoned Wash Fault, a north-northeast trending fault connecting the Abandoned Wash Fault and GDF, a north-northeast trending splay from Solitario Canyon Fault, the Sundance Fault, the Diabolous Ridge reverse fault, and a fault cutting the southeast end of Tonsil Ridge.[9, 10] These faults have displacements on the order of 5 m to >10 m. In addition, there are approximately 50 smaller faults with lengths of 10's to 100's of meters, mapped in the Tiva Canyon Tuff within the repository outline.

A primary control on water flow in stratified rocks is the difference in hydrologic properties of sequential rock layers. If the stratigraphic sequence is undeformed, this "vertical" inhomogeneity and anisotropy will dominate. In faulted strata, however, such as those at Yucca Mountain, geologic structures (faults and fractures) exert additional controls on flow:

(a) fault offsets alter the overall geometry of and communication between fault blocks,[17] (b) fault zones commonly form relatively impermeable barriers to cross-fault flow and permeable pathways for along-fault flow,[18, 19] (c) relatively small faults and fractures lead to permeability anisotropy in fault blocks,[20] and (d) fault and fracture conductivity (and permeability anisotropy) may be influenced by the *in situ* stress field.[21, 22]

Several recent studies have focused on fault zone deformation processes and resulting effects on the hydrological properties of the fault zones.[18, 23, 19, 21, 22] Fault zones in porous granular rock (e.g., nonwelded tuff such as the PTn)[24] may produce cataclastic grain-size reduction,[18] producing gouge zones or deformation bands (or deformation band swarms) that have lower permeability and porosity than the host rock.[18, 19] In contrast, fault zone deformation in densely lithified rocks (e.g., crystalline rocks, welded tuff, and other rocks characterized by high intergranular strength) may tend to produce coarse-grained breccias and wide fault damage zones with increased permeability relative to the host rock.[21] With increasing displacement, a lower permeability fault core may also develop within fault zones in densely lithified rocks.[19]

Fault zones within the welded or nonwelded tuff units at Yucca Mountain may affect flow because of the effects of fault-related deformation on hydrological properties. Faults that intersect the PTn unit may be of particular importance to flow in the unsaturated zone because of the potential of such faults to intercept lateral flow, resulting in focused vertical flow. Lateral flow along the PTn is expected considering the contrast in hydrologic properties between the PTn and the underlying TSw unit. The evidence, however, suggests that lateral down-dip flow of water through the PTn is limited to tens of meters before vertical breakthrough.[25] No perched water has been found, nor has any evidence of springs been found at exposed PTn bedding contacts. Several hypotheses have been suggested for the lack of persistent lateral flow and ponding. Flow through fractures in the PTn does not explain the lack of persistent lateral flow because matrix imbibition of water flowing in

fractures is strong in the PTn based on estimated hydrologic properties of the matrix and fractures.[26] Laterally, the PTn is a relatively uniform pyroclastic series of deposits with some local evidence of slight reworking.[27] Primary lateral variations in the PTn generally occur over large distances and thus cannot explain the lack of continuity of lateral flow.

The periodicity of breakthrough of flow through the PTn may be explained by considering that the unit may be intersected by several faults, potentially spaced on the order of tens of meters, with sufficient property contrast between the fault zone and host rock to intercept lateral flow and cause locally elevated vertical flux. An indirect evidence for the occurrence of elevated vertical flux in the vicinity of faults arises from anomalous concentrations of ^{36}Cl identified in matrix pore-water specimens collected from the Exploratory Studies Facility.[25, 28] Several matrix pore-water samples containing elevated ^{36}Cl values are spatially correlated with structural features like faults or intensely fractured zones, either with the surficial trace of the structural feature or the trace at depth. Some elevated ^{36}Cl values, however, show no such correlation. The authors believe that the correlation of ^{36}Cl values with faults would be improved by considering only faults that intersect the PTn. Numerical-model results are presented here to illustrate the potential effects of such faults on repository-level percolation flux.

MODEL DESCRIPTION

The model cross section (Fig. 1) was discretized into 3708 cells (nodes) for integrated finite difference analyses (Fig. 2). The cells are aligned parallel and normal to the model-layer interfaces, with approximate dimensions of 30 and 10 m in the layer-parallel and normal directions, respectively. The Ghost Dance Fault was not assigned special cells but is represented in the model as a contact between dissimilar materials.

Thermal-Hydrological Model

Thermal-hydrological behavior was simulated using the mass and energy transport (METRA) module of the thermal-hydrological-chemical simulation system MULTIFLO.[29] METRA uses an integrated finite difference spatial discretization to solve two-phase (water and air) flow and heat transport in fractured porous media. METRA was specifically designed for modeling strongly heated geological repositories and other geothermal systems. Unlike conventional groundwater simulation codes that consider the air phase to be a passive bystander in the flow process, METRA models explicitly the flow of water vapor and air and includes the effects of condensation and vaporization. Lookup tables provide accurate values for the thermodynamic properties of water and water vapor.

Flow in the fractured porous rock was simulated using a dual-continuum model (DCM) option. Flow and heat transport in the DCM option takes place in two overlapping continua: one representing the interconnecting fracture system and the other the host rock (matrix). Interchange between the two media is proportional to the potential difference between the two, including the effects of capillary pressure (p_c) on mass transfer in systems not fully saturated with water. The DCM option provides the capability for modeling nonequilibrium flow in fractures, in contrast to the equivalent continuum model (ECM), which presumes instantaneous thermodynamic equilibrium between the two continua.[6] The matrix porosity

(ϕ_m) and permeability (k_m) and the fracture porosity (ϕ_f) and permeability (k_f) vary among the model layers (Table I). In general, the fracture permeability is anisotropic with a vertical component (k_{fv}) that is larger than the horizontal component (k_{fh}). Anisotropy in the matrix permeability was assumed negligible.

Moisture retention properties are critical to modeling flow in unsaturated rock. The van Genuchten relationships[30] were used to relate capillary pressure to liquid saturation s_l for both continua:

$$|p_c| = \frac{1}{\alpha}\left\{\left(s^{eff}\right)^{-1/\lambda} - 1\right\}^{1/m} \tag{1}$$

Here, s_l^{eff} is the effective saturation:

$$s_l^{eff} = \left(s_l - s_l^r\right) / \left(s_l^0 - s_l^r\right) \tag{2}$$

where s_l^r is the residual saturation and s_l^0 is the maximum saturation. The relative permeability for liquid (k_{rl}) was modeled as

$$k_{rl} = \sqrt{s_l^{eff}}\left\{1 - \left[1 - \left(s^{eff}\right)^{1/\lambda}\right]^{\lambda}\right\}^2 \tag{3}$$

and the gas relative permeability (k_{rg}) was modeled as $k_{rg} = 1 - k_{rl}$.

The van Genuchten relationship involves two empirically determined parameters: α, which is related to the air-entry or bubbling pressure of the medium, and m, which controls the shape of the moisture-retention curve. The parameter λ is determined as $\lambda = 1 - 1/m$, a relationship frequently invoked for many classes of geologic material to allow for the use of Eq. (3) when the amount of relative permeability data is limited.[31] The values of α and m are significantly different for fractures and matrix; also both parameters vary between different model layers (Table II). In determining the flow between two adjacent nodes with differing hydrologic properties, upstream weighting was used to calculate the relative permeability, and harmonic averaging was used for the absolute permeability, a hybrid weighting for permeability that is standard for two-phase porous media flow systems.

Flow between fractures and matrix was calculated the same way, except that the unsaturated relative permeability from fractures to matrix was reduced by a factor A_f (Table II). The reduction factor accounts for the fact that only a fraction of the fracture surface is active (i.e., contains moisture) in unsaturated flow systems. A further refinement of this procedure for accounting for moisture distribution in fractures would be to represent A_f as a function of saturation. The treatment of A_f as a constant in this work is considered adequate because fracture saturations did not change significantly over the course of the simulations.

Simulation of thermal behavior was based on heat flow by conduction and convection, including the effects of vaporization and condensation. Conductive heat flow was modeled using bulk thermal properties (Table III), with bulk thermal conductivity, κ, determined as a function of s_l and the dry and saturated rock-mass thermal conductivities, κ_{dry} and κ_{sat}, respectively[32]:

$$\kappa = \kappa_{\text{dry}} + (\kappa_{\text{sat}} - \kappa_{\text{dry}})\sqrt{s_l} \tag{4}$$

Boundary and Initial Conditions

The boundary condition at the ground surface (top of model) consists of a constant infiltration flux and spatially variable but time-independent temperature and gas pressure. A mass flux equivalent to an infiltration rate of 10 mm/yr was applied, considering that estimates for the current averaged annual infiltration rate at Yucca Mountain lie in the range of 5–15 mm/yr.[1, 2, 3, 4, 5] The ground-surface temperature was determined as a function of elevation, z_e (m above sea level), using an equation obtained from regression analyses of Nevada State temperature data (S. Stothoff, personal communication):

$$T_{ma} = 21.667 - 0.006063 z_e \tag{5}$$

where T_{ma} is the mean annual temperature at the ground surface in °C. The atmospheric pressure P_a was also evaluated using an equation derived from regression analysis of Nevada

data (S. Stothoff, personal communication):

$$P_a = 29372 - 2.8494 z_e \tag{6}$$

which gives P_a in units of 0.001 in. of mercury.

The base of the model, z_e = 730 m, coincides with the water table. Consequently, the boundary condition at the base was set to a constant temperature of 30°C, which was established based on estimates of the average water-table temperature,[33] a saturation of 1.0, and atmospheric pressure of 92,486 Pa from Eq. (6). The east and west boundaries were assigned no-flow conditions.

The initial conditions were developed through transient analyses to steady state (starting with an arbitrary set of field variable values) using the specified thermal-hydrological properties (Tables I, II, and III) and boundary conditions. The results of such analyses are considered as the initial steady-state conditions.

Repository thermal loading was simulated as a time-decaying heat source applied over cells marked with dark dots in Fig. 2. The heat-source cells lie approximately along the horizontal broken line in Fig. 1, which represents the intersection of the proposed emplacement drifts with the model cross section. One design currently being considered for the proposed repository (referred to as the EDA-II design[34]) calls for 5.5-m-diameter emplacement drifts spaced at 81 m center-to-center (in a horizontal array) with waste packages placed end-to-end to give an initial average heat output of about 1.2 kW/m (of drift). The linear heat load decays with time to approximately 0.017 kW/m at 10 000 yr. This design corresponds to an areal thermal load equivalent of 60 tonnes U/acre (metric tons of uranium per acre). A time-decaying heat source strength with an initial value of about 1.2 kW/m was applied to each heat-source cell (Fig. 2). Because of the large cross-sectional area of each cell, about 300 m^2 compared to about 24 m^2 for an emplacement drift, the applied heat source is diluted by a factor of about 12 relative to the proposed thermal load design. As a result, the

calculated maximum temperatures at the source locations are expected to be lower than the anticipated maximum drift-wall temperatures.

Analysis Cases

Three sets of analyses were conducted. The first set consists of the base case, which examines the effects of stratigraphy, structural attitude, and geometric offset at the GDF (Fig. 1) on percolation-flux distributions and thermally driven moisture at the repository horizon. The base case uses the properties in Tables I, II, and III. The second analysis set examine the effects of a generic minor fault that intersects the PTn without necessarily producing a geometric offset of the unit. Such a generic fault was represented through a modification of hydrologic properties for one column of PTn cells across the entire thickness of the unit. The specific changes of the hydrologic properties are discussed later. The third analysis set examines the effects of a laterally discontinuous thermal-mechanical altered zone at the repository horizon through changes in the fracture porosity and permeabilities within the zone. The specific changes are discussed later.

Hydrologic Properties of a Generic Minor Fault

The values of fault-zone hydrologic parameters, such as ϕ, k, α, and m for both matrix and fractures, are required to model the effect of a small fault crossing the PTn. No direct data are available for the values of these parameters for fault zones in nonwelded tuffs at Yucca Mountain. Therefore, the parameter values are estimated in this work by modifying the corresponding ambient values for the PTn. The type and magnitude of the applied modifications were determined through examination of published work on measurements in fault zones in poorly lithified sediments.

A discussion of the features of fault zones in poorly lithified sediments[35] noted the occur-

rence of a general grain-size reduction resulting from combinations of several mechanisms: (a) deformation-induced mixing of clays with framework grains, (b) pressure solution, (c) cataclasis, (d) clay smear, and (d) cementation. These changes will lead to reductions in ϕ, k, and α. Permeability reductions of three to four orders of magnitudes for faults with discrete slip bands and up to two orders of magnitude for homogeneous faults have been reported.[35] Large permeability and porosity reductions were measured for sandstones at Moab, Utah,[18, 23] in deformation bands, zones of deformation bands, and slip planes associated with faults. The study[18] noted that the intensity of cataclasis and the clay content of the host rock control the magnitude of permeability reduction. A porosity reduction of one order of magnitude and permeability reduction of three orders of magnitude relative to the host rock were measured for the deformation bands (Table IV).

Similar results were obtained from laboratory and field measurements of hydraulic properties in directions parallel and perpendicular to small faults at two sites in the Rio Grande Rift basin of New Mexico[36] (Table IV). At both sites, the fault zone exhibited a wide range of permeability values while the undeformed areas exhibited a narrow range, giving a bimodal distribution of measured permeabilities in the damaged or mixed zones. The low-permeability population was interpreted as representing the areas with grain-size reduction and the high-permeability population was associated with pods of less deformed sediments.[36]

These results indicate that the porosity and permeability of the PTn rock unit (non-welded volcanic tuff similar to poorly lithified sediments) may decrease by about one and three orders of magnitude, respectively, between the relatively undeformed host rock and deformed zones associated with faulting. Information about the effect of faulting on the van Genuchten parameters may be developed by associating faulting-induced particle-size changes with a shift in the particle-size classification category of the affected sediment. Then the van Genuchten parameters may be estimated from hydrologic property values for the soil classification category taken from the literature.[37] Using this scheme, the particle-size

changes observed at the Moab site, for example, may be likened to a shift in particle-size category from loamy sand to clay loam. Such a change would correspond to a two-order and one-order of magnitude decrease in permeability and van Genuchten α, respectively.

Thermal-Mechanical Effects on Hydrologic Properties

A change in fracture aperture may result either from an increase or decrease in the fracture-normal stress (normal deformation response) or from the dilation of an individual fracture or a fracture network owing to fracture slip. The normal deformation response is considered elastic in that the associated aperture change is generally recoverable upon reversal of the stress change.[38, 39] On the other hand, fracture slip and the associated dilation are inelastic processes. Heat generated by repository thermal load is expected to cause an increase in compressive stress because of supressed thermal expansion of the rock, but the compressive stress will slowly decrease as the heat dissipates. As a result, fractures oriented normal to the thermally induced compressive stresses will experience a decrease in aperture that is expected to recover as the heat dissipates. Furthermore, fracture slip may occur in areas where the shear component of the induced stress is sufficient to overcome the shear resistance of fractures, and the associated dilation (fracture-aperture increase) is not reversible.

Because of the geometry of the proposed emplacement area (i.e., horizontal dimensions on the order of kilometers and a vertical dimension of only a few meters), the maximum compressive stress from repository thermal loading is expected to be horizontal, whereas the minimum compressive stress will be vertical.[40] Therefore, vertical and near-vertical fractures are expected to experience decrease in aperture owing to thermally induced compressive stress. The expected magnitude of aperture change will vary depending on the magnitude of compressive stress increment and can be estimated from test data.[38, 39] A key aspect of the

proposed EDA-II design[34] is the close indrift packing of waste packages with large interdrift separation, which is expected to give a relatively high temperature at the drift wall that decreases rapidly to a lower temperature in the interdrift pillars. The associated maximum compressive stress is expected to be relatively high near the drifts but decrease with distance from the drift wall. As a result, the occurrence of appreciable decrease in vertical-fracture aperture is expected to be limited to zones close to the drifts. Therefore, such zones will be laterally discontinuous. The fracture-aperture decrease within such zones is expected to be reversible as the repository heat dissipates. Existing laboratory data[38, 39] suggest that the vertical fracture apertures within such zones may decrease to about 70 percent of their preemplacement values and increase again thereafter.

The magnitudes of fracture-aperture increase associated with the inelastic response of a rock mass are more difficult to estimate. Although the dilation response of individual fractures can be characterized through laboratory testing,[38, 39] increase in fracture aperture associated with the inelastic response of a rock mass is a product of the fracture-network characteristics and less dependent on the behavior of individual fractures.[41] Considering that the inelastic deformation of a fractured rock is contributed almost entirely by movement on fractures, it can be shown that the fracture-porosity change, $\Delta\phi_f$, associated with the inelastic deformation of a rock element is equal to the inelastic volumetric strain, ε^{N}. For a regularly fractured rock element with fixed fracture aperture, b, and spacing, d, in three mutually perpendicular directions, the fracture porosity and aperture can be shown to be related as follows:

$$\phi_{fo} = \frac{3b_o}{d} \qquad \text{and} \qquad \Delta\phi_f = \frac{3\Delta b}{d} \tag{7}$$

where ϕ_{fo} and b_o are the initial fracture porosity and aperture, respectively, and Δb is the fracter-aperture change. Using these relationships, it can be shown that the aperture-change

ratio, R_b, and the fracture-porosity change ratio, R_ϕ, are related as follows:

$$R_b = 1 + \frac{\Delta b}{b_o} = R_\phi = 1 + \frac{\Delta \phi_f}{\phi_{fo}} = 1 + \frac{\varepsilon^{\mathrm{N}}}{\phi_{fo}} \tag{8}$$

Therefore, the ratio R_b can be calculated from the inelastic volumetric strain with the initial fracture porosity or aperture. It is worth noting that the fracture-permeability change ratio, $R_k = k_f/k_{fo}$ (k_{fo} is the initial fracture permeability), can be related to R_b using the relationship between fracture permeability and aperture,[42, 43] which results in

$$k_f = \frac{b^3}{12d} \quad \Longrightarrow \quad R_k = R_b^3 = \left(1 + \frac{\varepsilon^{\mathrm{N}}}{\phi_{fo}}\right)^3 \tag{9}$$

A series of continuum thermal-mechanical analyses was conducted using a drift-scale model to examine potential R_b distributions from thermal-mechanical response of the proposed repository rock mass. Results from the analyses (e.g., Fig. 3) indicate that the intensity of thermally induced fracture dilation is spatially variable. The thermal-mechanical analyses, based on a two-dimensional (plane-strain) model, were conducted using ABAQUS, a commercially available finite element code.[44] The model (e.g., Fig. 3) extends vertically from a depth of 350 m below the drift axis to the ground surface at 320 m above the drift axis. It extends 40.5 m horizontally from the center of the drift to the middle of the interdrift pillar, which gives a drift center-to-center spacing of 81 m as specified in the EDA-II design.[34] The drift is represented by a semicircular hole with a diameter of 5.5 m. The analyses followed a sequentially coupled thermal-mechanical procedure[44]: a heat-conduction analysis was performed to generate temperature histories that were used as input in a mechanical analysis. The material properties and boundary conditions for the heat conduction and mechanical analyses are given in Tables V and VI.

The results indicate that fracture dilation is greatest in the immediate vicinity of the opening and in the center of the interdrift pillar. The values of R_b are up to 10 in the pillar center and greater than 10 in the drift area, which correspond to R_k values of up

to 1000 in the pillar center and greater than 1000 in the drift area. The dominant orientations of the dilating fractures may be obtained from discontinuum thermal-mechanical modeling, in which rock fractures are represented explicitly. For example, Fig. 4 indicates dominant orientations of thermally induced fracture slip at Yucca Mountain that vary from subhorizontal in the RMQ5 rock-mass category (most competent rock) to subvertical in the RMQ1 (least competent rock) category.[45] This pattern of predicted geomechanical response for Yucca Mountain, which is consistent with results reported previously,[40, 46] arises because the response is stress-controlled in the RMQ5 rock-mass category, such that the orientation of slip is determined by the orientation of thermally induced stress. On the other hand, response is structure-controlled in the RMQ1 rock-mass category, where slip follows the exposed preexisting structural weaknesses in the rock irrespective of the stress orientation.

Previous studies on the effects of faults on groundwater flow have shown that faults favorably oriented for slip in the ambient stress field tend to be the most active groundwater flow pathways.[22, 47, 48] This observation has been explained by increased small-scale fracturing and faulting in the vicinity of faults on the verge of shear failure.[47] Slip on a preexisting fracture or fault generates movement on neighboring fractures, resulting in a dilation zone that follows the dominant fracture-slip orientation. Therefore, the orientation of dilation zones associated with thermally induced fracture slip follows the pattern illustrated in Fig. 4 (i.e., subhorizontal in RMQ5 rock-category areas and subvertical in RMQ1 areas).

The information presented in this section indicates that geomechanical response to thermal loading in a fractured rock mass would lead to the development of hydrologically altered zones that are laterally discontinuous. The altered zones are characterized by increased aperture of horizontal fractures and a net increase or decrease in aperture of vertical fractures. Existing data on stress-induced fracture closure[38, 39] and the results presented here on fracture dilation suggest that R_b values may vary from approximately 0.7 to >10 for vertical fractures and from 1.0 to >10 for horizontal fractures. An altered zone with these charac-

teristics was incorporated in the thermal-hydrological model by modifying the aperture of vertical and horizontal fractures within a zone that extends approximately 160 m laterally and approximately 25 m above and below the repository axis. Different combinations of R_b values for vertical and horizontal fractures were investigated as discussed later.

INITIAL STEADY-STATE MOISTURE FLOW: BASE CASE

The vertical profiles of matrix saturations at the initial steady state reflects the occurrence of welded and nonwelded rock units (Fig. 5). Matrix saturations are generally 0.9–1.0 in the welded units and approximately 0.5–0.7 in the nonwelded. Measured matrix saturations from Yucca Mountain exploratory boreholes close to the model section (e.g., UZ16, SD7, and SD12)[33] show the same general pattern. An important difference between the measured saturation profiles[33] and the calculated profiles (Fig. 5) is that the transition from PTn saturations of 0.5–0.7 to TSw saturations of 0.9–1.0 occurs more rapidly (over approximately the top 40 m of the TSw) in the calculated profiles. The same transition occurs over about 100 m of the TSw unit in the measured saturation profiles.[33] This difference may be related to the lumping of the PTn subunits into a single unit, which was necessitated by model discretization.

The GDF and the PTn-TSw contact have important effects on repository-level vertical flux as shown in Fig. 6. Flux entering the PTn is diverted laterally over an area of approximately 150 m wide near the up-dip (i.e., west) boundary of the model domain. Vertical flux is reduced (relative to the input flux) in this area, increases back to the input value of 10 mm/yr throughout most of the PTn on the west side of the GDF, and increases at the up-dip side of the GDF. The vertical flux on the up-dip side of the GDF increases because the lateral flux in the PTn unit is interrupted by the GDF where the nonwelded PTn unit is juxtaposed against the welded TSw unit on the down-dip side (Fig. 1). These features of the vertical flux profile are consistent with theoretical analyses of model systems involving capillary diversion along sloping layers.[49] On the up-dip side of the system, vertical flux is diverted to lateral flux because of the effects of a capillary barrier against moisture flow from the PTn to the TSw. The zone of reduced vertical flux is limited, however. The saturation in the PTn increases from west to east (down dip) in this zone (Fig. 6), with a corresponding

decrease in capillary pressure. After approximately 150 m, the capillary pressure in the PTn becomes too small to prevent moisture flow into the underlying TSw unit, and the vertical flux returns to the input value of 10 mm/yr.

The repository-level vertical flux follows the same pattern: reduced flux (relative to the input infiltration flux) within the diversion zone, flux close to the input infiltration rate over most of the repository area, and elevated flux close to and on the up-dip side of the GDF. The elevated vertical flux on the up-dip side of the GDF is consistent with results from previous studies.[6, 33] As was discussed earlier (in *Geologic Features Important to Flow*), several other major intrablock faults that cut through the repository block can be expected to produce similar effects on repository-level vertical flux.

The role of capillarity contrasts as the dominant mechanism for lateral diversion in the PTn is important because of the implication that lateral diversion in the PTn cannot be relied on to support an argument for reduced percolation flux (relative to the infiltration flux) throughout the proposed repository block. The results from a previous study[33] that indicate repository-level percolation fluxes are generally lower than the infiltration flux over the repository area may need to be reexamined. Results from the current study (e.g., Fig. 6) indicate that the repository-level percolation flux is equal to or greater than the infiltration flux over most of the repository area, except for the diversion zone near the upstream boundary.

Effects of Minor Faults in the PTn Unit

The effects of an altered zone in the PTn caused by a generic minor fault that intersects the unit without necessarily producing measurable offset were investigated. The fault zone was represented by the vertical ellipse in Fig. 2. The reduction factors applied to the matrix porosity, van Genuchten α, and horizontal and vertical fracture aperture are given in

Table VII. The matrix permeability was reduced by the square of the matrix-porosity factor and the fracture permeability by the cube of the corresponding aperture factor. Hence, the reduction factors of 0.1 for b_h and 1.0 for b_v (Table VII) imply a reduction factor of 0.001 for horizontal fracture permeability and 1.0 (no change) for vertical fracture permeability. Such fracture-permeability change combined with the isotropic matrix permeability produced a permeability anisotropy that is consistent with the observation that fault zones commonly form relatively impermeable barriers to cross-fault flow and permeable pathways for along-fault flow.[18, 19]

Three cases were analyzed as described in Table VII, in addition to the base case (representing the response of the system without the changes described in Table VII). The resulting profiles of percolation flux along the PTn (Fig. 7) indicate that the fault zone acted as a lateral-flow barrier in the first two cases ($\phi/10$ and $\phi/2$ cases) but as a conduit in the third case ($\phi/2 + \alpha/10$ case). For the first two cases, lateral flow is decreased relative to the base case and is close to zero on the upstream side of the fault intersection. For the third case, lateral flow is increased relative to the base case on the upstream side but is negative with a greater magnitude than the base case on the downstream side. As a result, water flows laterally toward the fault from both the downstream and upstream sides.

On the other hand, the effect of the fault on vertical flux at the repository depth follows the same pattern in all three cases: an increase in flux magnitudes on the upstream side of the fault and a decrease on the downstream side (Fig. 7). A fault intersecting the PTn would cause focused vertical flux at the repository horizon, irrespective of whether the fault acts as a flow barrier or a conduit. Both major faults associated with a significant offset of the PTn (such as the GDF) and minor faults that may often be ignored because of not producing measurable offset can be expected to produce similar effects on repository-level percolation flux (compare Figs. 6 and 7). A flux magnification factor of up to 2.5–3.0 was obtained from the models, but this factor can change, depending on the fault-zone properties and possibly

the infiltration rate.

Effects of a Generic Thermal-Mechanical Altered Zone

The effects of a generic thermal-mechanical altered zone, represented by the horizontal ellipse in Fig. 2, were investigated by changing the apertures of horizontal and vertical fractures as described in Table VIII. The fracture permeabilities consistent with the modified fracture apertures were determined using Eq. (9). The applied combinations of horizontal-fracture dilation and net vertical-fracture closure or dilation can be expected from various combinations of elastic and inelastic response as indicated in Table VIII. As explained earlier, the dilation of horizontal fractures is anticipated to result from inelastic response in areas of high rock-mass quality, dilation of vertical fractures from inelastic response in low rock-mass quality areas, and closure of vertical fractures from elastic response in areas of high stress. Therefore, the specific combination of fracture opening and closure response that may occur in a given area depends on the rock-mass quality and whether the rock-mass response is elastic or inelastic.

Six cases were analyzed, representing different combinations of horizontal-fracture dilation and vertical-fracture closure or dilation (Table VIII). In all cases, fracture dilation or closure resulted in a redistribution of vertical flux magnitudes within the altered zone (Figs. 8 and 9). The closure of vertical fractures tends to divert flux to the outside of the altered zone, while the dilation of horizontal fractures tends to divert flux to the downstream side, but within the perimeters, of the altered zone. If horizontal-fracture dilation and net vertical-fracture closure occur simultaneously, as may be expected over the roofs of drifts in high rock-mass quality (such as RMQ5) areas (Fig. 4), the effects of horizontal-fracture dilation on flow would be dominant. For example, the $10b_h$-and-b_v case (representing horizontal-fracture dilation with no change in vertical fractures) and the $10b_h$-and-$0.1b_v$

case (representing horizontal-fracture dilation with vertical-fracture closure) gave essentially identical results (Fig. 9). Both cases resulted in elevated vertical flux within and on the downstream side of the altered zone, indicating that the effect of horizontal-fracture dilation would be dominant irrespective of the magnitude of simultaneous vertical-fracture closure within a closure ratio of 1.0–0.1. A flux magnification factor of up to 4.0 was obtained from the models, but the value of this factor depends on the magnitudes and orientation of fracture dilation or closure and possibly on the geometry of the altered zone and the infiltration rate.

Effects on Thermally Driven Moisture Flow

The temperature and saturation profiles from the base case with thermal load (Fig. 10) indicate that above-boiling temperatures and dry conditions would prevail at the repository level for 500 to 1000 yr. Matrix saturations return to the ambient values by about 1000 yr, but high temperatures are maintained at the repository level for a much longer time. The 10 000-yr temperature profile shows temperatures significantly higher than the ambient (preemplacement) values. This combination of high temperature and high saturation would imply elevated humidities in the emplacement drifts for much of the period of regulatory concern.

The rate of rewetting (i.e., matrix saturations returning to ambient values after a dry period) is influenced by focused moisture flow. Results presented earlier in this paper demonstrate that focused moisture flux may result from fault zones that intersect the PTn or from thermal-mechanical altered zones that may develop following waste emplacement. The saturation histories in Fig. 11 indicate that areas subjected to focused moisture flux would rewet faster than other areas. Although the dryout rate appears not to be influenced significantly by focused moisture flow, the rate of rewetting is significantly affected. In the results in

Fig. 11, matrix saturation returned to its ambient value of about 0.98 at about 500 yr for the node that is under focused moisture flux and about 1000 yr for the neighboring node. Therefore, emplacement drifts in areas of focused moisture flux would not only experience high humidities for longer periods but would also be more likely to experience dripping (water seeping into drifts) because of the availability of increased quantities of water.

IMPORTANCE TO REPOSITORY ISSUE RESOLUTION

The Nuclear Regulatory Commission (NRC) has embarked on a prelicensing program for the proposed Yucca Mountain repository that focuses on developing information toward the resolution of key technical issues (KTIs) considered critical to repository performance.[8] Each KTI is divided into subissues with reduced technical scope to facilitate incremental resolution. Information in this paper will help establish the technical bases for specific subissues in two KTIs: thermal effects on flow (TEF) and repository design and thermal-mechanical effects (RDTME).

One subissue in the TEF KTI addresses the sufficiency of the DOE thermohydrologic modeling approach to predict the nature and bounds of thermal effects on flow in the near field.[50] The aspects of the technical scope of this subissue addressed in this paper include (a) effects of discrete geologic features, such as faults and fractures; (b) lateral movement of moisture (derived either from surface infiltration or from condensation); (c) effects of heterogeneity of media properties; and (d) effects of coupled processes. Related questions are addressed in a second TEF subissue that deals with the abstractions used to account for thermal effects on flow in the DOE total system performance assessment. The subissue requires that the abstracted model used to predict water influx into an emplacement drift must be demonstrated to reproduce the lower- and upper-bound process-level predictions of water influx into a drift. Thermal-mechanical effects on flow into emplacement drifts are also considered in a subissue of the RDTME KTI with specific emphasis on changes in hydrological properties associated with thermal-mechanical response of the rock mass.[40]

Percolation flux has a significant effect on drift seepage in that the likelihood of water influx into drifts and the magnitude of such influx increase as the percolation flux increases.[51] The results discussed in this paper illustrate that discrete geologic features, such as faults that intersect the PTn, are potential locations for focused percolation flux at the repository

horizon. As a result, drifts located in such areas would experience higher likelihoods and magnitudes of water influx. Furthermore, because of lateral flow within thermal-mechanical altered zones, emplacement drifts on the downstream side of and within such altered zones are likely to receive elevated percolation flux. Therefore, the occurrence of faults in the PTn, including those faults that may be ignored because of their failure to produce measurable offset, needs to be considered in the prediction of water influx into emplacement drifts. Also, thermal-mechanical altered zones (including their rate of development and geometrical and hydrological characteristics) have been shown to be essential to repository-level percolation flux and, consequently, the influx of water into emplacement drifts.

CONCLUSIONS

In this paper, numerical-modeling results are presented to examine the effects of discrete geologic features and thermal-mechanical altered zones on the distributions of percolation flux and thermally driven moisture at the proposed repository horizon at Yucca Mountain. Thermal-hydrological flow was simulated using a series of two-dimensional site-scale models. The geometrical and hydrological characteristics of thermal-mechanical altered zones were developed through separate thermal-mechanical modeling. The percolation flux through the unsaturated zone has significant effects on (a) the occurrence and magnitude of water influx into the emplacement drifts, (b) the onset and rates of waste package corrosion, (c) the mobilization of waste into aqueous states, and (d) the transport of radionuclides to the saturated zone. The following observations are presented:

1. Areas of the repository close to and on the up-dip side of faults that intersect the PTn experience relatively high percolation flux. Such faults intercept lateral flux in the PTn and redirect the flux vertically because of contrasts in hydrologic properties between the fault zone and the surrounding host rock. The fault may act either as a flow barrier or conduit because of the property contrast, but the effect on repository-level percolation flux is the same in both cases. Relatively large faults (such as the GDF) and smaller faults that may be ignored because of their failure to produce measurable stratigraphic offset may produce the same effect on repository-level percolation flux, depending on the fault-zone property contrast.

2. Thermal-mechanical altered zones are likely to be laterally discontinuous, being localized around emplacement drifts and in the middle of interdrift pillars. The type, magnitude, and orientation of the fracture-aperture change associated with such zones depend on the rock-mass quality and on whether rock-mass response is elastic or inelastic. Elastic response is associated with vertical-fracture closure, while inelastic response is associated with

horizontal-fracture dilation in high rock-mass quality areas and vertical-fracture dilation in areas of low rock-mass quality.

3. Lateral flow within thermal-mechanical altered zones results in redistribution of percolation flux, with elevated vertical flux occurring on the downstream side of the altered zone. Flux is diverted from altered zones characterized by vertical-fracture closure. Horizontal-fracture dilation appears to have the dominant effect on flux, always causing elevated flux within and on the downstream side of the altered zone.

4. Elevated percolation flux appears to have little effect on dryout rates, but the rewetting of dryout zones within elevated-flux areas is relatively accelerated. Consequently, emplacement drifts located in areas of elevated flux would experience longer periods of wetness and elevated humidity.

Predictions of (a) the onset and rates of water influx into emplacement drifts and (b) the temporal variation of relative humidity within the drifts are essential in the assessment of the long-term performance of the proposed Yucca Mountain repository. Results discussed in this paper indicate that models used to perform such predictions need to consider (a) the location of an emplacement drift relative to faults that intersect the PTn; and (b) the development, geometry, and hydrological characteristics of thermal-mechanical altered zones.

ACKNOWLEDGEMENTS

The work described in this paper was performed at the Center for Nuclear Waste Regulatory Analyses (Southwest Research Institute, San Antonio, Texas) for the U.S. Nuclear Regulatory Commission (NRC) under contract number NRC-02-97-009. The work was done on behalf of the NRC Office of Nuclear Material Safety and Safeguards, Division of Waste Management. The views expressed in the paper are those of the authors and do not necessarily reflect the views or regulatory position of the NRC. The authors are grateful to D. Sims, R. Green, B. Sagar, J. Pryor, B. Long, C. Patton, and L. Selvey for contributions

made at various stages of the project.

References

1. "Viability Assessment of a Repository at Yucca Mountain. Volume 1: Introduction and Site Characteristics," DOE/RW-0508/V1, U.S. Department of Energy, Office of Civilian Radioactive Waste Management (1998).

2. J. A. HEVESI and A. L. FLINT, "Geostatistical Model for Estimating Precipitation and Recharge in the Yucca Mountain Region, Nevada–California," Water Resources Investigation Report 96-4123, U.S. Geological Survey (1996).

3. A. L. FLINT, J. A. HEVESI, and L. E. FLINT, "Conceptual and Numerical Model of Infiltration for Yucca Mountain Area, Nevada," Water Resources Investigation Report, U. S. Geological Survey (1996).

4. A. C. BAGTZOGLOU, N. M. COLEMAN, E. C. PEARCY, S. A. STOTHOFF, and G. W. WITTMEYER, "Unsaturated and Saturated Flow Under Isothermal Conditions," *NRC High-Level Radioactive Waste Program FY96 Annual Progress Report*, B. SAGAR, Ed., NUREG/CR-6513, U.S. Nuclear Regulatory Commission (1996).

5. S. A. STOTHOFF, "Sensitivity of Long-Term Bare Soil Infiltration Simulations to Hydraulic Properties in an Arid Environment," *Water Resour. Res.*, **33**, *4*, 547–558 (1997).

6. G. I. OFOEGBU, A. C. BAGTZOGLOU, R. T. GREEN, and M. A. MULLER, "Effects of Perched Water on Thermally Driven Moisture Flow at the Proposed Yucca Mountain Repository for High-Level Waste," *Nucl. Technol.*, **125**, 235–253 (1999).

7. "Near-Field/Altered Zone Coupled Effects Expert Elicitation Project," Civilian Radioactive Waste Management System Management and Operating Contractor (1998).

8. B. SAGAR, Ed., "NRC High-Level Radioactive Waste Program Annual Progress Report: Fiscal Year 1996," NUREG/CR–6513, No. 1, U.S. Nuclear Regulatory Commission (1997).

9. W. C. DAY, C. J. POTTER, D. SWEETKIND, R. P. DICKERSON, and C. A. SAN JUAN, "Bedrock Geologic Map of the Central Block Area, Yucca Mountain, Nye County, Nevada," Miscellaneous Investigation Series Map I–2601, scale 1:6,000, U.S. Geological Survey (1998).

10. W. C. DAY, R. P. DICKERSON, C. J. POTTER, D. S. SWEETKIND, C. A. SAN JUAN, R. M. DRAKE, II, and C. J. FRIDRICH, "Bedrock Geologic Map of the Yucca Mountain Area, Nye County, Nevada," Miscellaneous Investigation Series Map I–2627, scale 1:24,000, U.S. Geological Survey (1998).

11. "Viability Assessment of a Repository at Yucca Mountain. Volume 2: Preliminary Design Concept for the Repository and Waste Package," DOE/RW-0508/V2, U.S. Department of Energy, Office of Civilian Radioactive Waste Management (1998).

12. "Geologic Framework Model (GFM3.1)," Analysis and Modeling Report MDL-NBS-GS-000002 REV 00 ICN 01, U.S. Department of Energy, Office of Civilian Radioactive Waste Management (2000).

13. J. HINDS, T. M. BANDURRAGA, M. A. FEIGHNER, and Y. S. WU, "Geology of the Unsaturated Zone and the UZ Model," *The Site-Scale Unsaturated Zone Model of Yucca Mountain, Nevada for the Viability Assessment*, G. S. BODVARSSON, T. M. BANDURRAGA, and Y. S. WU, Eds., LBNL-40376, Lawrence Berkeley National Laboratory (1997).

14. E. L. HARDIN, Ed., "Near-Field/Altered-Zone Models Report," UCRL-ID-129179, Lawrence Livermore National Laboratory (1998).

15. D. A. FERRILL, J. A. STAMATAKOS, and D. SIMS, "Normal Fault Corrugation: Implications for Growth and Seismicity of Active Normal Faults," *J. Struct. Geol.*, **21**, 1027–1038 (1999).

16. D. A. FERRILL and A. P. MORRIS, "Extensional Relay Ramp Deformation," *J. Struct. Geol.*, In Review.

17. U. S. ALLAN, "Model for Hydrocarbon Migration and Entrapment Within Faulted Structures," *Am. Assoc. Pet. Geol. Bull.*, **73**, *7*, 803–811 (1989).

18. M. ANTONELLINI and A. AYDIN, "Effect of Faulting on Fluid Flow in Porous Sandstones: Petrophysical Properties," *Am. Assoc. Pet. Geol. Bull.*, **78**, *3*, 355–377 (1994).

19. J. S. CAINE, J. P. EVANS, and C. B. FORSTER, "Fault Zone Architecture and Permeability Structure," *Geology*, **24**, 1025–1028 (1996).

20. D. A. FERRILL, A. P. MORRIS, J. A. STAMATAKOS, and D. SIMS, "Crossing Conjugate Normal Faults," *Am. Assoc. Pet. Geol. Bull.*, **84**, *10* (2000).

21. J. P. EVANS, C. B. FORSTER, and J. V. GODDARD, "Permeability of Fault-Related Rocks and Implications for Hydraulic Structure of Fault Zones," *J. Struct. Geol.*, **19**, 1393–1404 (1997).

22. D. A. FERRILL, J. WINTERLEE, G. WITTMEYER, D. SIMS, S. COLTON, A. ARMSTRONG, and A. P. MORRIS, "Stressed Rock Strains Groundwater at Yucca Mountain, Nevada," *GSA Today*, **9**, *5*, 1–8 (1999).

23. M. ANTONELLINI and A. AYDIN, "Effect of Faulting on Fluid Flow in Porous Sandstones: Geometry and Spatial Distribution," *Am. Assoc. Pet. Geol. Bull.*, **79**, *5*, 642–671 (1995).

24. D. S. SWEETKIND, E. R. VERBEEK, J. K. GESLIN, and T. C. MOYER, "Fracture Character of the Paintbrush Tuff Nonwelded Hydrologic Unit, Yucca Mountain, Nevada," Administrative Report to U.S. Department of Energy, U. S. Geological Survey (1995).

25. "Unsaturated Zone Flow Model Expert Elicitation Project," MOL.19971009.0582, U.S. Department of Energy, Office of Civilian Radioactive Waste Management (1997).

26. L. E. FLINT, A. L. FLINT, C. A. RAUTMAN, and J. D. ISTOK, "Physical and Hydrologic Properties of Rock Outcrop Samples at Yucca Mountain, Nevada," Open-File Report 95-280, U.S. Geological Survey (1996).

27. T. C. MOYER, J. K. GESLIN, and L. E. FLINT, "Stratigraphic Relations and Hydrologic Properties of the Paintbrush Tuff Nonwelded (PTn) Hydrologic Unit, Yucca Mountain, Nevada," Open-File Report 95-397, U.S. Geological Survey (1996).

28. J. T. FABRYKA-MARTIN, A. V. WOLFSBERG, S. S. LEVY, K. CAMPBELL, P. TSENG, J. L. ROACH, and L. E. WOLFSBERG, "Evaluation of Flow and Transport Models of Yucca Mountain, Based on Chlorine-36 Studies for FY98," Yucca Mountain Project Milestone Report SP33DDM4, Los Alamos National Laboratory (1998).

29. P. C. LICHTNER, M. S. SETH, and S. PAINTER, "MULTIFLO User's Manual, MULTIFLO Version 1.2: Two-Phase Nonisothermal Coupled Thermal-Hydrological-Chemical Flow Simulator," Center for Nuclear Waste Regulatory Analyses (2000).

30. M. Th. VAN GENUCHTEN, "A Closed-Form Equation for Predicting the Hydraulic Conductivity of Unsaturated Soils," *Soil Scien. Soci. Amer. Jour.*, **44**, 892–898 (1978).

31. M. Th. VAN GENUCHTEN, F. J. LEIJ, and S. R. YATES, "The RETC Code for Quantifying the Hydraulic Functions of Unsaturated Soils," EPA/600/2-91/065, Office of Research and Development, U.S. Environmental Protection Agency (1991).

32. W. H. SOMERTON, A. H. EL-SHAARANI, and S. M. MOBARAK, "High Temperature Behavior of Rocks Associated with Geothermal-Type Reservoirs," *Proceedings, 44th Annual California Regional Meeting of the Society of Petroleum Engineers*, SPE-4897. Society of Petroleum Engineers (1974).

33. Y. S. WU, C. HAUKWA, and G. S. BODVARSSON, "A Site-Scale Model for Fluid and Heat Flow in the Unsaturated Zone of Yucca Mountain, Nevada," *Journal of Contaminant Hydrology*, **38**, 185–215 (1999).

34. "License Application Design Selection Report," B00000000-01717-4600-00123, Rev. 01, TRW Environmental Safety Systems, Inc. (1999).

35. Q. J. FISHER and R. J. KNIPE, "Fault Sealing Processes in Siliciclastic Sediments. In Faulting, Fault Sealing and Fluid Flow in Hydrocarbon Reservoirs," G. JONES, Q. J. FISHER, and R. J. KNIPE, Eds., Geological Society Special Publication, No. 147, 117–135. Geological Society (1999).

36. J. M. SIGDA, L. B. GOODWIN, P. S. MOZLEY, and J. L. WILSON, "Permeability Alteration in Small-Displacement Faults in Poorly Lithified Sediments: Rio Grande Rift, Central New Mexico," *Faults and Subsurface Fluid Flow in the Shallow Crust*, W. C. HANEBERG, Ed., Geophysical Monograph, No. 113, 51–68. American Geophysical Union (1999).

37. R. F. CARSEL and R. S. PARRISH, "Developing Joint Probability Distributions of Soil Water Retention Characteristics," *Water Resour. Res.*, **24**, *5*, 755–769 (1988).

38. N. BARTON, S. BANDIS, and K. BAKHTAR, "Strength, Deformation and Conductivity Coupling of Rock Joints," *Int. J. Rock Mech. Min. Sci. & Geomech. Abstr.*, **22**, *3*, 121–140 (1985).

39. S. M. HSIUNG, D. D. KANA, M. P. AHOLA, A. H. CHOWDHURY, and A. GHOSH, "Laboratory Characterization of Rock Joints," NUREG/CR–6178, U.S. Nuclear Regulatory Commission (1994).

40. "Issue Resolution Status Report. Key Technical Issue: Repository Design and Thermal-Mechanical Effects, Rev. 2," Division of Waste Management, Office of Nuclear Material Safety and Safeguards, U.S. Nuclear Regulatory Commission (1999).

41. R. CHEN, "Analyses of Drift Stability and Rockfall Due to Earthquake Ground Motion at Yucca Mountain, Nevada," *Rock Mechanics for Industry: Proceedings, 37th U.S. Rock Mechanics Symposium*, B. AMADEI, R. L. KRANZ, G. A. SCOTT, and P. H. SMEALLIE, Eds., **2**, 759–766, A. A. Balkema, Rotterdam (1999).

42. D. ELSWORTH and C. R. MASE, "Chapter 8: Groundwater in Rock Engineering," *Comprehensive Rock Engineering*, J. A. HUDSON, Ed., **1**, 201–226, Pergamon Press, New York (1993).

43. J. S. Y. WANG and D. ELSWORTH, "Permeability Changes Induced by Excavation in Fractured Tuff," *Rock Mechanics for Industry: Proceedings, 37th U.S. Rock Mechanics Symposium*, B. AMADEI, R. L. KRANZ, G. A. SCOTT, and P. H. SMEALLIE, Eds., **2**, 751–757, A. A. Balkema, Rotterdam (1999).

44. "ABAQUS User's Manual, Version 5.8," Hibbit, Karlsson & Sorensen, Inc., Pawtucket, RI (1998).

45. R. CHEN, G. I. OFOEGBU, and S. HSIUNG, "Modeling Drift Stability in Fractured Rock at Yucca Mountain, Nevada—Discontinuum Approach," *Proceedings, 4th North American Rock Mechanics Symposium*, A. A. Balkema, Rotterdam, 2000.

46. G. I. OFOEGBU, "Variations of Drift Stability at the Proposed Yucca Mountain Repository," *Rock Mechanics for Industry: Proceedings, 37th U.S. Rock Mechanics*

Symposium, B. AMADEI, R. L. KRANZ, G. A. SCOTT, and P. H. SMEALLIE, Eds., **2**, 767–773, A. A. Balkema, Rotterdam (1999).

47. C. A. BARTON, M. D. ZOBACK, and D. MOOS, "Fluid Flow Along Potentially Active Faults in Crystalline Rock," *Geology*, **23**, 683–686 (1995).

48. T. FINKBEINER, C. A. BARTON, and M. D. ZOBACK, "Relationships Among In-Situ Stress, Fractures and Faults, and Fluid Flow: Monterey Formation, Santa Maria Basin, California," *Am. Assoc. Pet. Geol. Bull.*, **81**, 1975–1999 (1997).

49. B. ROSS, "The Diversion Capacity of Capillary Barriers," *Water Resour. Res.*, **27**, *8*, 2155–2156 (1991).

50. "Issue Resolution Status Report. Key Technical Issue: Thermal Effects on Flow, Rev. 2," Division of Waste Management, Office of Nuclear Material Safety and Safeguards, U.S. Nuclear Regulatory Commission (1999).

51. "Viability Assessment of a Repository at Yucca Mountain. Volume 3: Total System Performance Assessment," DOE/RW-0508/V3, U.S. Department of Energy, Office of Civilian Radioactive Waste Management (1998).

Table I: Hydrologic Parameters for the Base Model[14]

Model Layer Number	Model Layer Name	Hydro-geologic Unit	ϕ_f (10^{-4} Units)	k_{fh} (10^{-13} m^2)	k_{fv} (10^{-13} m^2)	ϕ_m	k_m (10^{-17} m^2)
1	tcw12	TCw	2.99	60.3	138.	0.066	0.540
2	ptn	PTn	0.484	5.25	5.25	0.369	1610.
3	tsw32	TSw	1.29	7.08	151.	0.146	18.2
4	tsw33	TSw	1.05	8.91	263.	0.135	2.04
5	tsw34	TSw	1.24	4.27	67.6	0.089	0.408
6	tsw35	TSw	3.29	9.12	38.0	0.115	2.22
7	tsw36	TSw	3.99	12.0	12.0	0.092	0.870
8	ch2vc	CHn	0.714	2.88	2.88	0.321	5500.
9	pp3vp	CHn	0.714	6.92	7.08	0.274	191.
10	pp2zp	CHn	0.110	0.646	0.251	0.197	1.75
11	bf3vp	CHn	0.714	6.92	7.08	0.274	191.
12	bf2zp	CHn	0.110	0.646	0.251	0.197	1.75

Table II: Van Genuchten Fitting Parameters for the Base Model[14]

Model Layer Name	s_{lf}^r	λ_f	α_f (10^{-3} Pa^{-1})	s_{lm}^r	λ_m	α_m (10^{-6} Pa^{-1})	A_f (10^{-4} Units)
tcw12	0.01	0.669	2.37	0.13	0.2447	2.01	5.00
ptn	0.01	0.667	0.913	0.10	0.3859	34.3	5020.
tsw32	0.01	0.667	1.42	0.04	0.2861	20.0	5.00
tsw33	0.01	0.667	1.73	0.06	0.2479	6.21	5.00
tsw34	0.01	0.643	0.934	0.18	0.3212	1.19	12.3
tsw35	0.01	0.667	1.26	0.08	0.1983	4.01	5.00
tsw36	0.01	0.667	1.32	0.18	0.5138	0.808	5.00
ch2vc	0.01	0.667	1.18	0.06	0.2291	41.2	5000.
pp3vp	0.01	0.667	1.42	0.07	0.3142	16.6	5.00
pp2zp	0.01	0.667	1.14	0.18	0.3568	8.39	5000.
bf3vp	0.01	0.667	1.42	0.07	0.3142	16.6	5.00
bf2zp	0.01	0.667	1.14	0.18	0.3568	8.39	5000.

Table III: Bulk (Rock-Mass) Thermal Parameters for the Base Model[14]

Name	ρ (kg/m^3)	C_m [J/(kg·K)]	κ_{dry} [J/(s·m·K)]	κ_{sat} [J/(s·m·K)]
tcw12	2510.0	837.0	1.28	1.88
ptn	2340.0	1080.0	0.35	0.50
tsw32	2550.0	866.0	1.06	1.62
tsw33	2510.0	883.0	0.71	1.80
tsw34	2530.0	948.0	1.56	2.33
tsw35	2540.0	900.0	1.20	2.02
tsw36	2560.0	865.0	1.42	1.84
ch2vc	2240.0	1200.0	0.58	1.17
pp3vp	2580.0	841.0	0.66	1.26
pp2zp	2510.0	644.0	0.74	1.35
bf3vp	2580.0	841.0	0.66	1.26
bf2zp	2510.0	644.0	0.74	1.35

Table IV: Permeability and Porosity Reductions in Fault Zones That Intersect Poorly Lithified Sediments

Measurement Site	Permeability k (darcy)		Porosity ϕ	
	Host Rock	Fault Zone	Host Rock	Fault Zone
Moab[23]	0.6–5.0	0.002–0.01	0.17–0.22	0.01–0.05
Santa Ana[36]	3.0–46	0.01–7	0.28	0.16–0.24
Elmendorf[36]	4.0–12	0.2–8.0	0.25	0.17
1 darcy $\approx 10^{-12}$ m^2				

Table V: Heat Conduction Analysis Model

Boundary conditions	Symmetry on vertical boundaries; fixed temperature 18.7°C at top and 34.3°C at base.
Thermal load	Decays with time from 1.2 kW/m (of drift) to 0.017 kW/m at 10 000 yr. Distributed uniformly over drift cross-sectional area.
Thermal conductivity	2.13 W/m·K
Density	2210 kg/m^3
Specific heat capacity	Varies with temperature to account for water evaporation and condensation, with values of 969, 4741, 4741, and 988 J/kg·K at temperature of $\leq$ 92°, 96°, 112°, and $\geq$ 116°C, respectively.

Table VI: Continuum Mechanical Analysis Model with Temperature Change

Boundary conditions	Symmetry on vertical boundaries; free surface at top and no vertical displacement at base.
Young's modulus	32.6 GPa
Poisson's ratio	0.21
Thermal expansivity	Temperature dependent, with values of 7.14, 9.07, 9.98, 11.74, 13.09, and 15.47 (10^{-6}/K) at temperatures of $\leq$ 50°, 100°, 125°, 150°, 175°, and 200°C, respectively.
Friction angle	34.4°
Dilation angle	17.2°
Cohesion	Varies with time to represent mechanical degradation, with values of 5.08 MPa at 0–50 yr and 2.54 MPa at 100 yr and later.
Initial fracture porosity	10^{-4} (Used to calculate R_b)

Table VII: Reduction Factors Applied to PTn Hydrologic Parameters to Define a Generic Fault Zone and the Resulting Repository-Level Flux Magnification

	Reduction Factors				
Case Name	for ϕ_m	for α_m	for b_h	for b_v	Flux Magnification
$\phi/10$ case	0.1	1.0	0.1	1.0	2.5
$\phi/2$ case	0.5	1.0	0.5	1.0	1.5
$\phi/2 + \alpha/10$ case	0.5	0.1	0.5	1.0	2.6
ϕ_m, α_m, b_h, and b_v are matrix porosity and van Genuchten α and horizontal and vertical fracture aperture, respectively					

Table VIII: Fracture-Aperture Change Ratios Applied to Define a Thermal-Mechanical Altered Zone and the Resulting Flux Magnification

R_{bh}	R_{bv}	Flux Magnification	Remarks
1.0	10^{-1}	4.0	All elastic, high stress
1.0	$10^{-0.5}$	1.5	All elastic, relaxing stress
$10^{0.5}$	1.0	1.25	Inelastic and elastic
10.0	10^{-1}	2.5	Inelastic and elastic
10.0	1.0	2.25	Inelastic and elastic
10.0	10.0	1.25	All inelastic
$R_b = 1+\Delta b/b_o$; subscripts h and v represent horizontal and vertical, respectively.			

List of Figure Captions

1 Model domain: an east-west vertical section through Yucca Mountain. Circled numbers represent the model stratigraphic names as defined in Table I.

2 Finite difference discretization of the model domain. Cells used for heat-source application are marked with dark dots. Two ellipses with dashed boundaries represent generic geomechanically altered zones: a fault zone intersecting the PTn represented by the subvertical ellipse centered at about $(860, -240)$, and a thermal-mechanical altered zone represented by the horizontal ellipse centered at about $(500, -434)$.

3 Fracture-aperture change ratio R_b $(= b/b_o = R_k^{1/3})$ from continuum thermal-mechanical analysis of a drift-scale model of the proposed Yucca Mountain repository. Only the part of the model within 50 m above and below the repository axis is shown. There was no change in fracture aperture (i.e., $R_b = 1$) outside this zone.

4 Distributions of fracture shear displacement from discontinuum thermal-mechanical analyses using drift-scale models of the proposed Yucca Mountain repository. Dotted lines represent individual fractures; dark lines represent shear displacement, with line thickness proportional to shear-displacement magnitude. RMQ5 is the most competent rock-mass category, whereas RMQ1 is the least competent. Additional information about the model is provided in a separate publication.[45]

5 Vertical profiles of matrix saturation at horizontal distances of 450, 1200, and 1600 m from the west model boundary. Broken lines represent the interfaces between welded and nonwelded tuff units. The profiles represent the initial steady-state moisture distribution (before waste emplacement) calculated using the base-case model.

6 Profiles of matrix saturation and vertical and lateral fluxes at mid-depth of the PTn unit, and vertical percolation flux at the repository depth, illustrating the effects of PTn-TSw contrast, stratigraphic dip, and major faults such as the GDF on deep percolation. The PTn profiles include only the part of the PTn on the west side of the GDF (Fig. 1).

7 Profiles of percolation flux at the mid-depth of the PTn unit and at the repository depth, illustrating the effects of a generic fault zone that intersects, but does not necessarily offset, the PTn. Lateral flux is positive in the direction of increasing horizontal distance.

8 Profiles of percolation flux at the repository depth, illustrating the effects of a generic thermal-mechanical altered zone. The results represent the effects of horizontal-fracture dilation with no change in vertical fractures and vertical-fracture closure with no change in horizontal fractures. Both cases are compared with the base case for which there is no change in fracture aperture.

9 Profiles of percolation flux at the repository depth, illustrating the effects of a generic thermal-mechanical altered zone. The results represent the effects of combining horizontal-fracture dilation with different magnitudes of net vertical-fracture dilation and closure. Parameters b_h and b_v represent the horizontal and vertical fracture apertures for the base-case

10 Vertical profiles of temperature and matrix saturation from the base-case model with thermal loading. Profiles represent the behavior at a horizontal distance of 450 m from the west model boundary.

11 Histories of temperature and saturation illustrating the effects of focussed water flux from a generic minor fault in the PTn. Taken from a thermal-load case that includes the PTn fault zone as illustrated in Fig. 2. Solid and broken-line curves are for the seventh and sixth heat-source nodes (counting from the east), respectively.

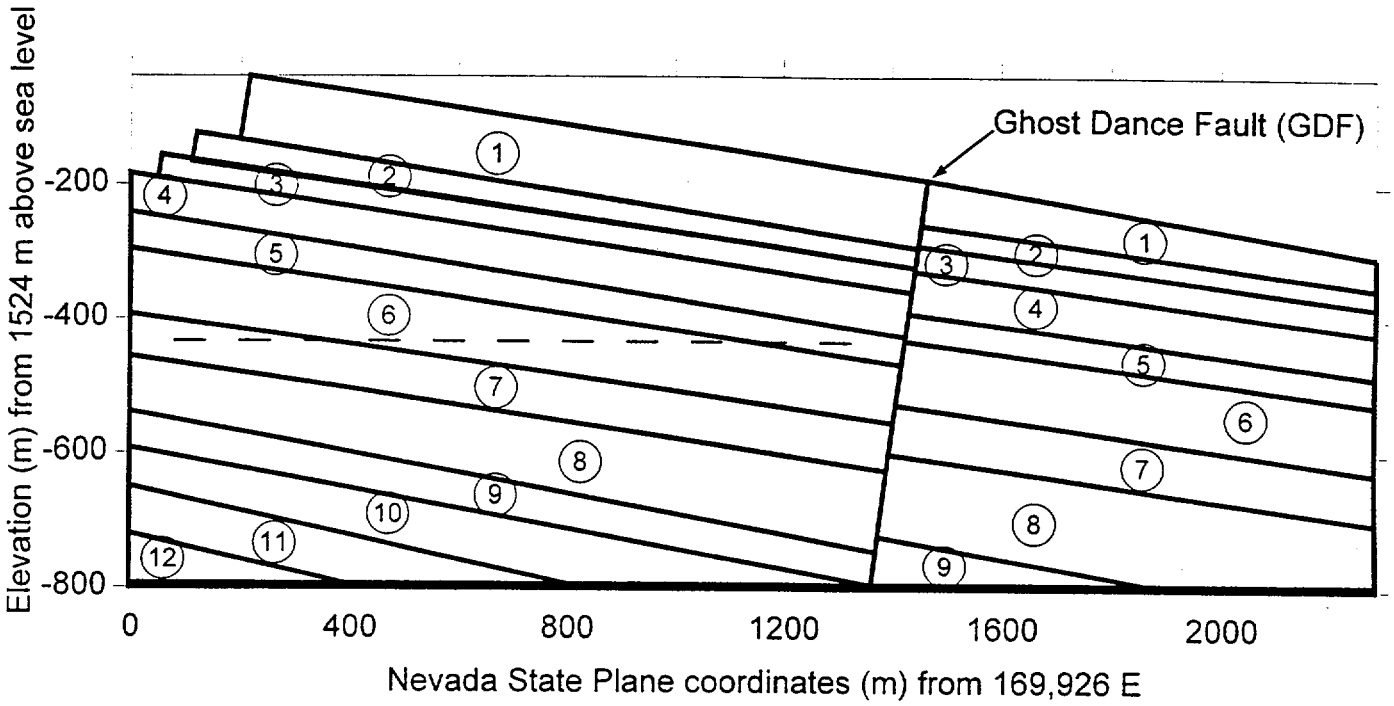

Ofoegbu et al., Fig. 1

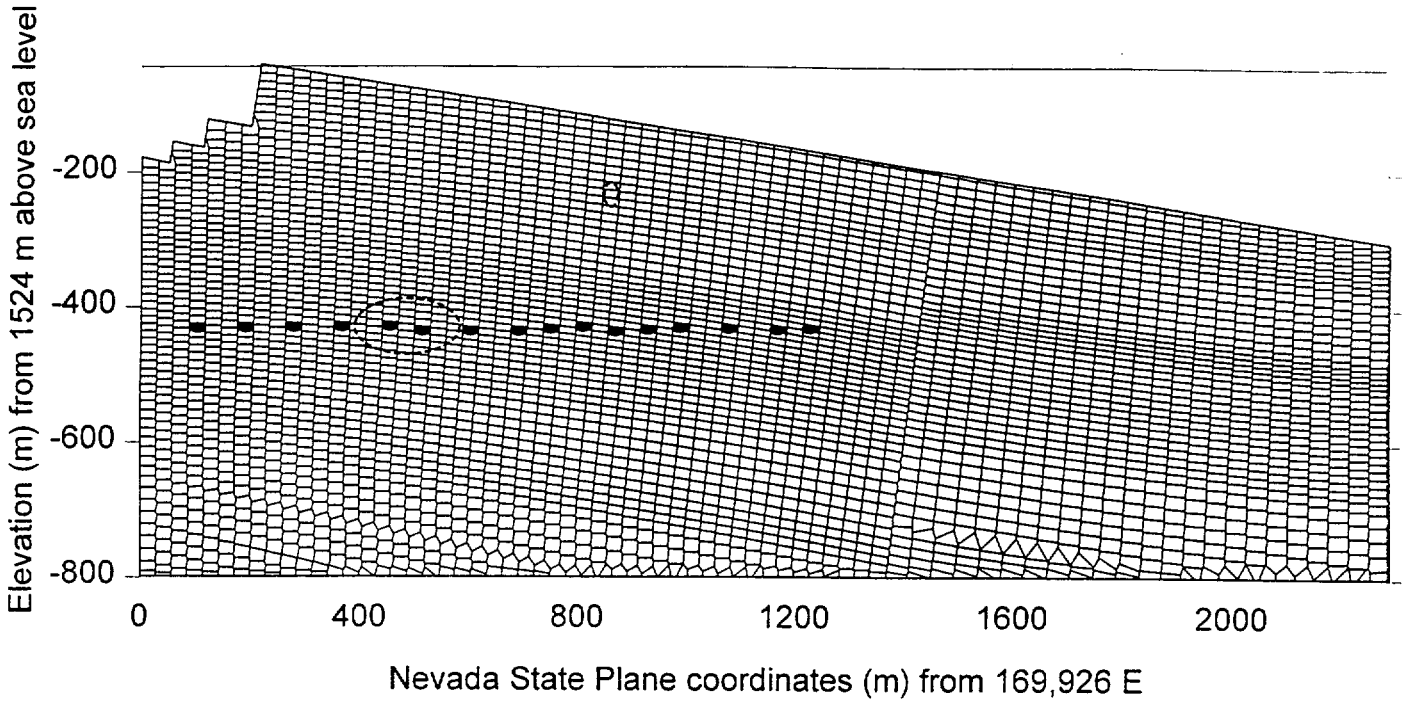

Ofoegbu et al., Fig. 2

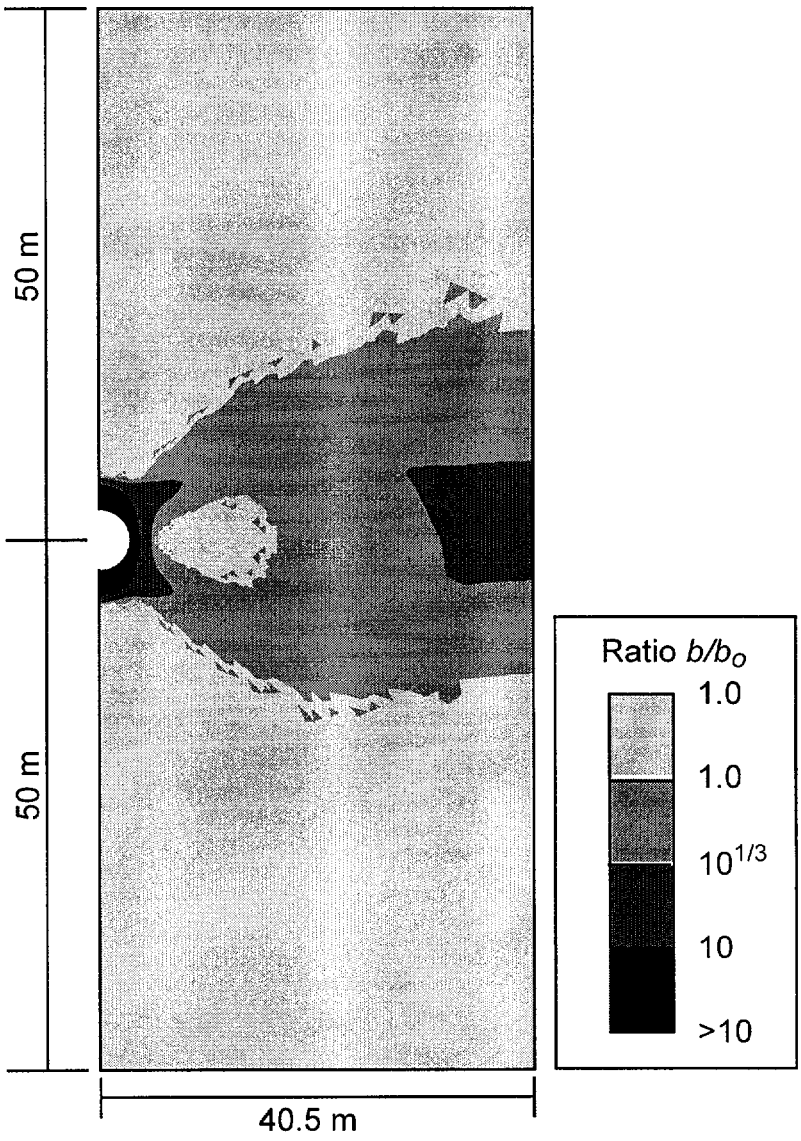

Ofoegbu et al., Fig 3

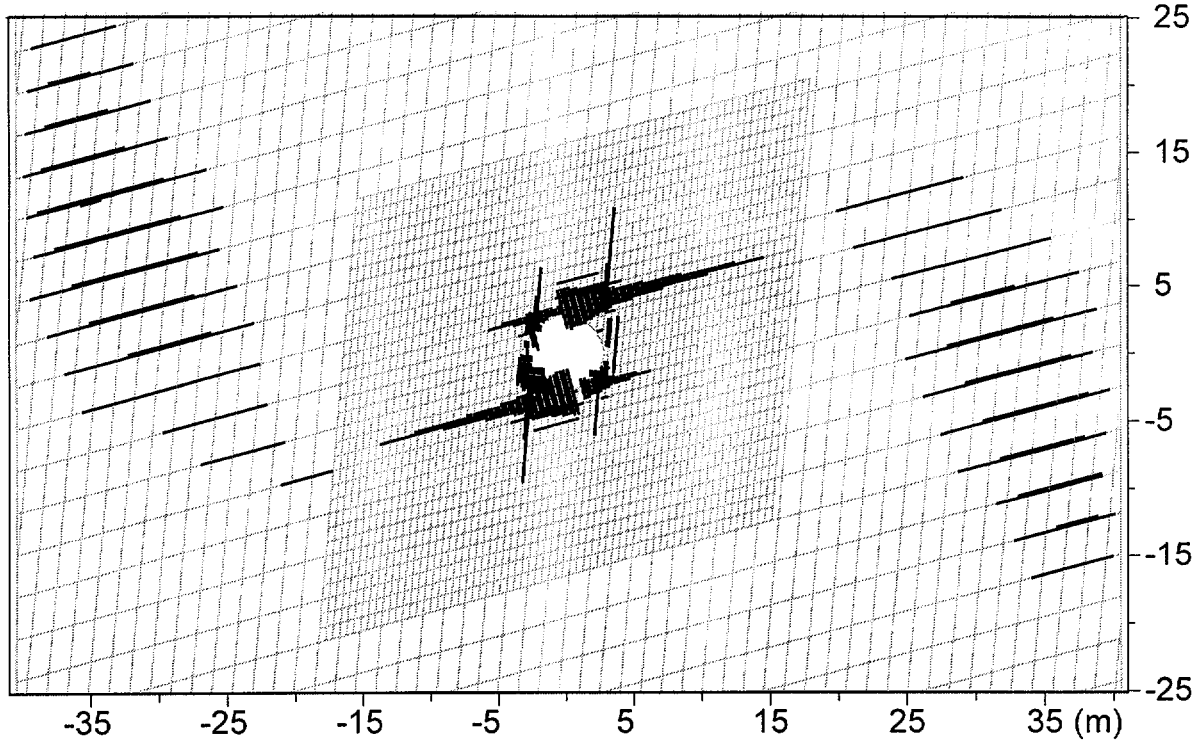
25
15
5
-5
-15
-25
-35
-25
-15
-5
5
15
25
35 (m)

(a) RMQ5

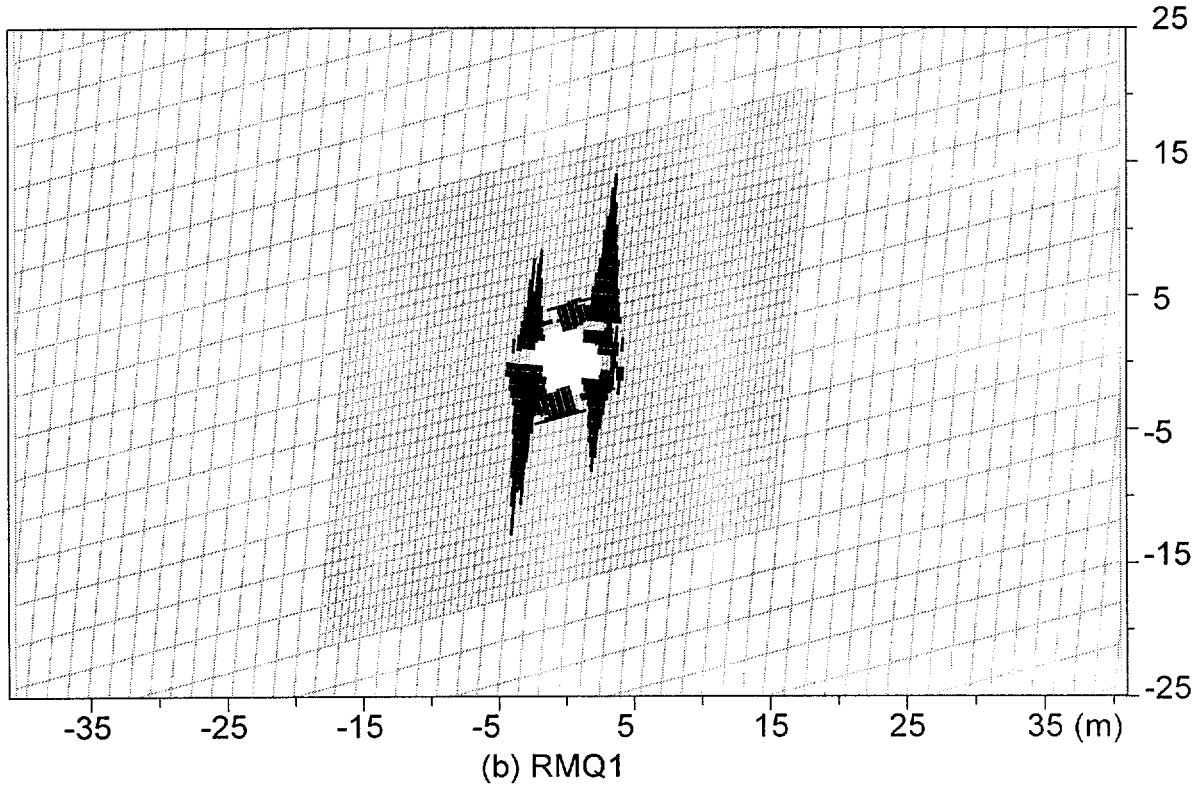
25
15
5
-5
-15
-25
-35
-25
-15
-5
5
15
25
35 (m)

(b) RMQ1

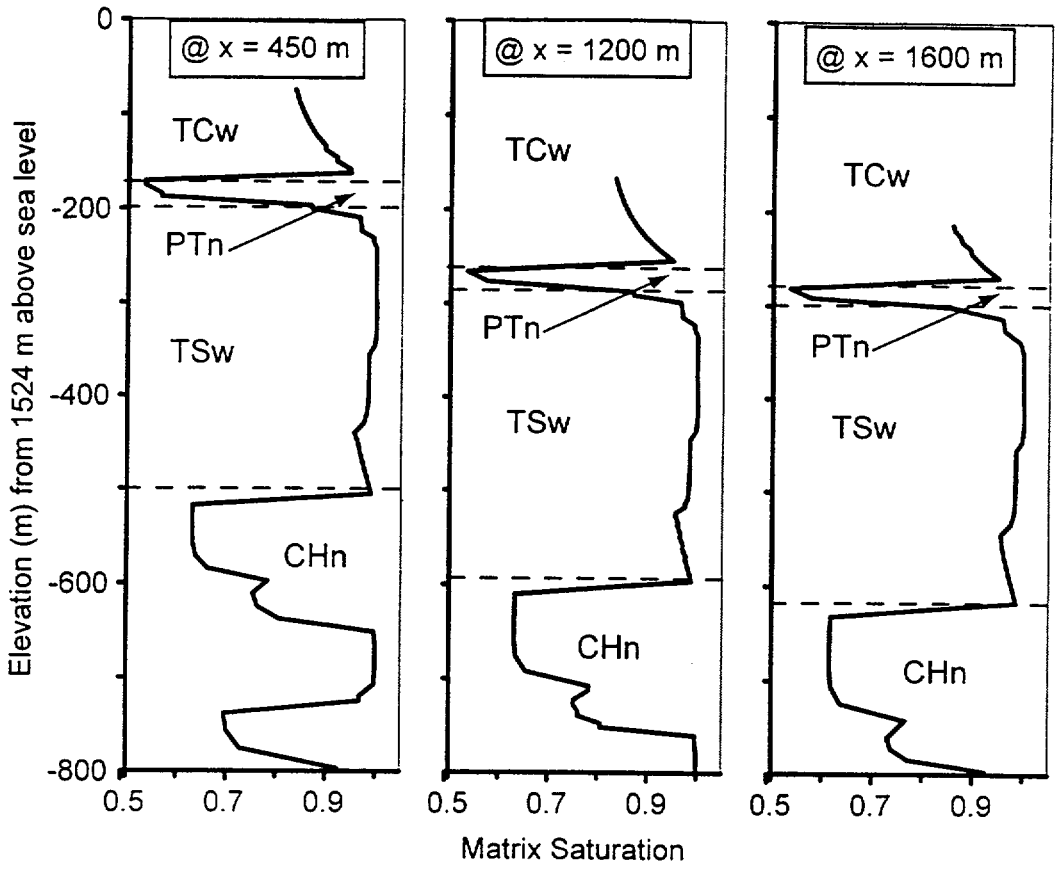

Ofoegbu et al., Fig. 5

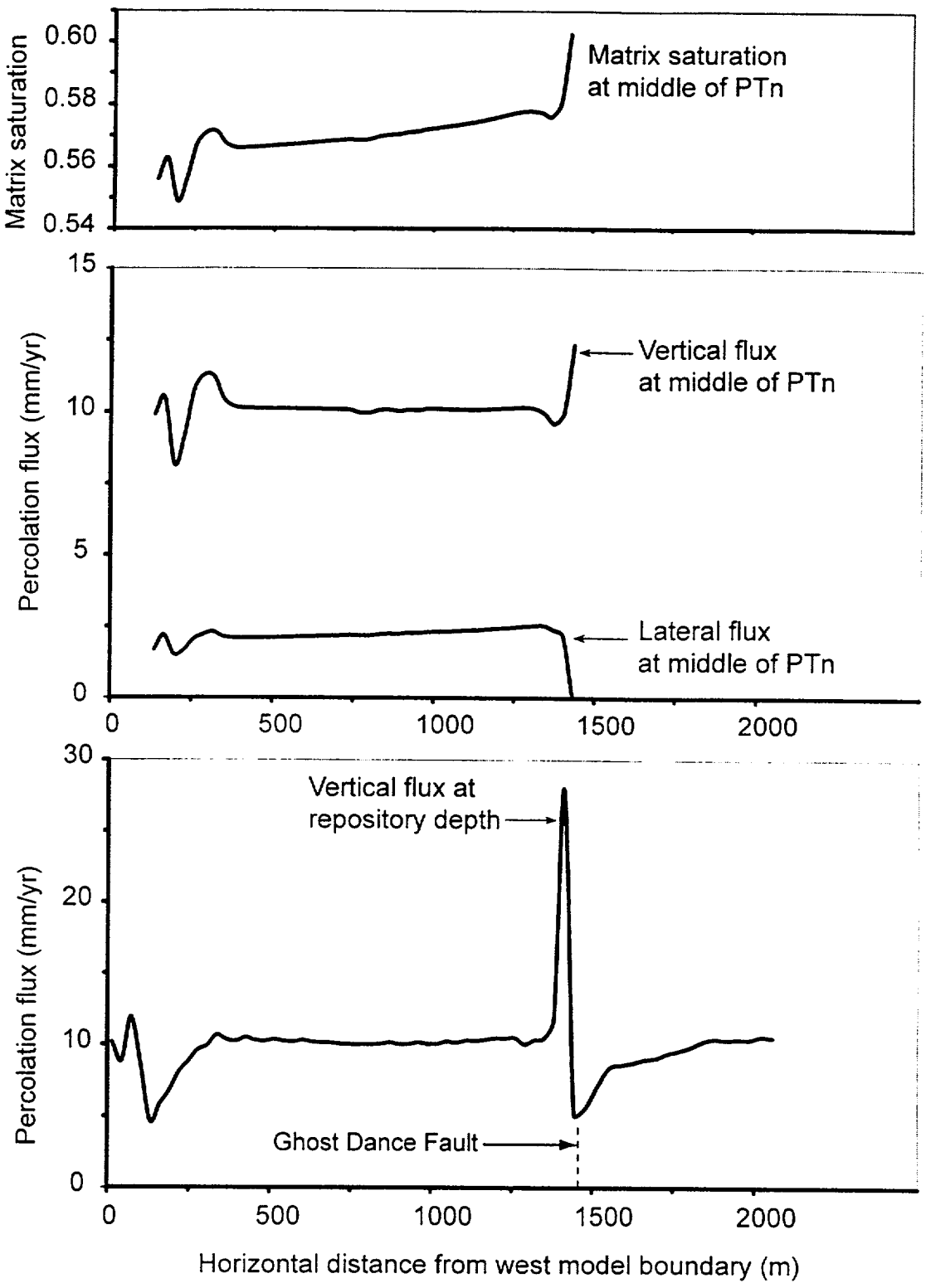

Ofoegbu et al., Fig 6

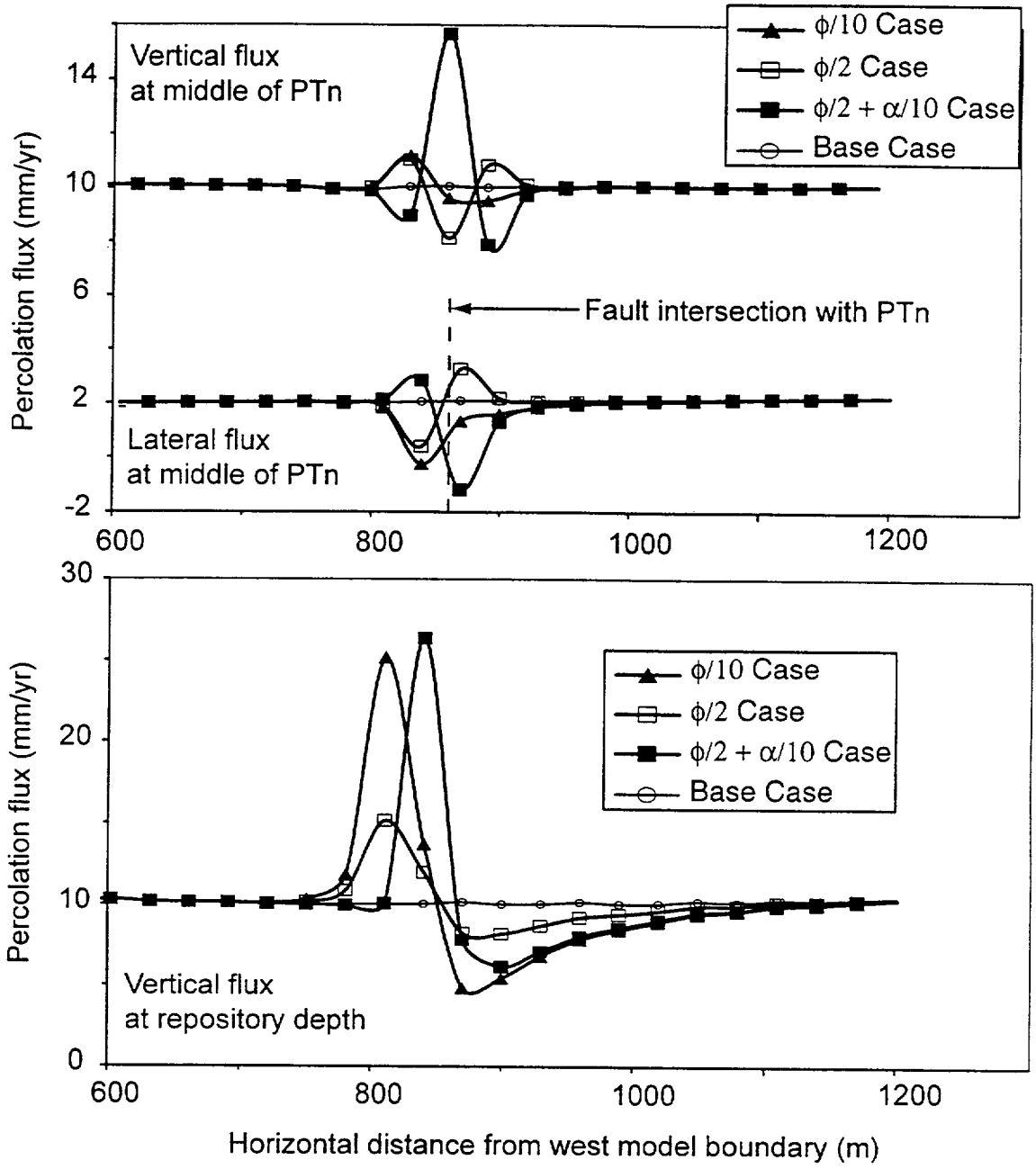

Ofoegbu et al., Fig 7

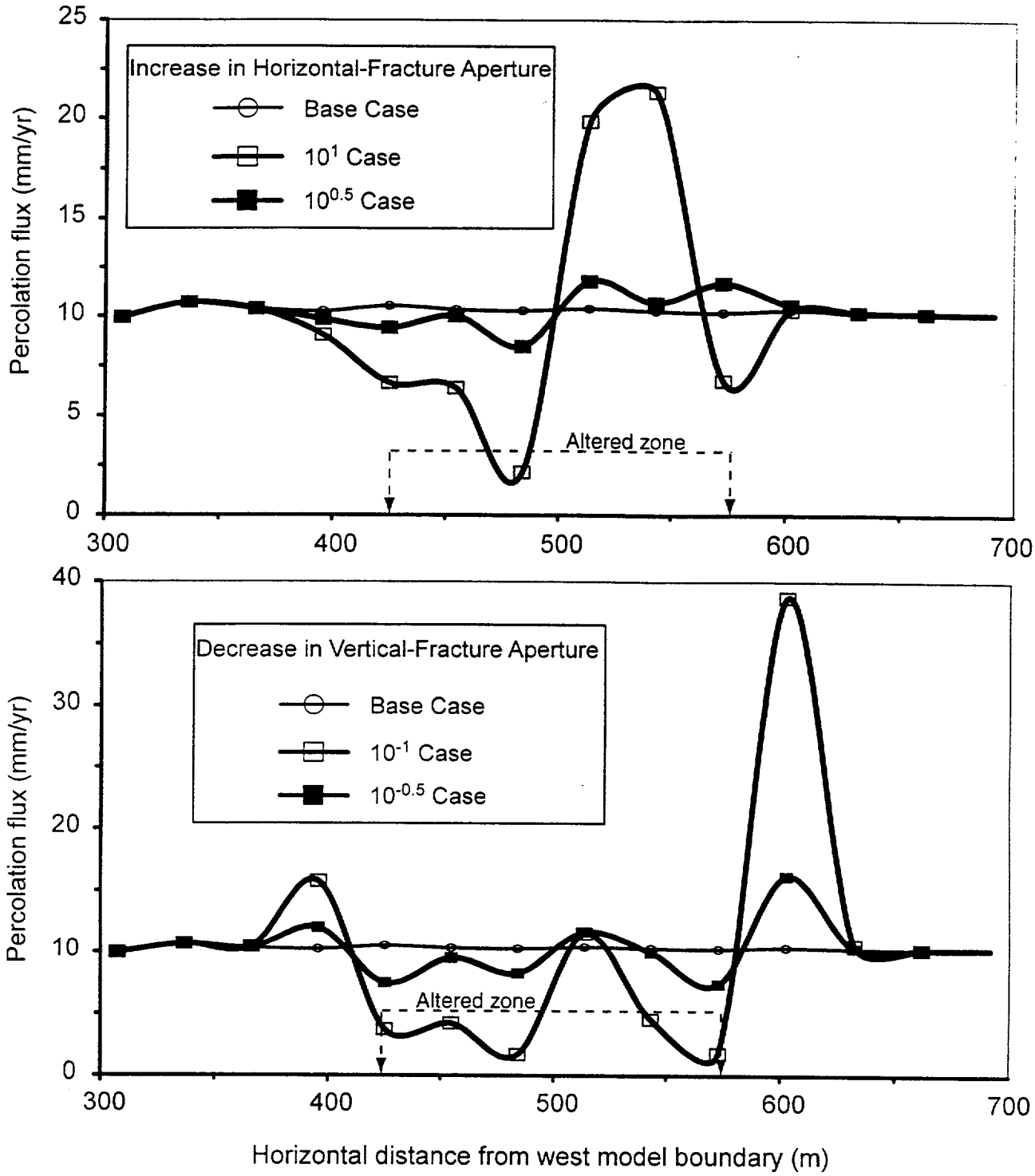

Ofoegbu et al., Fig 8

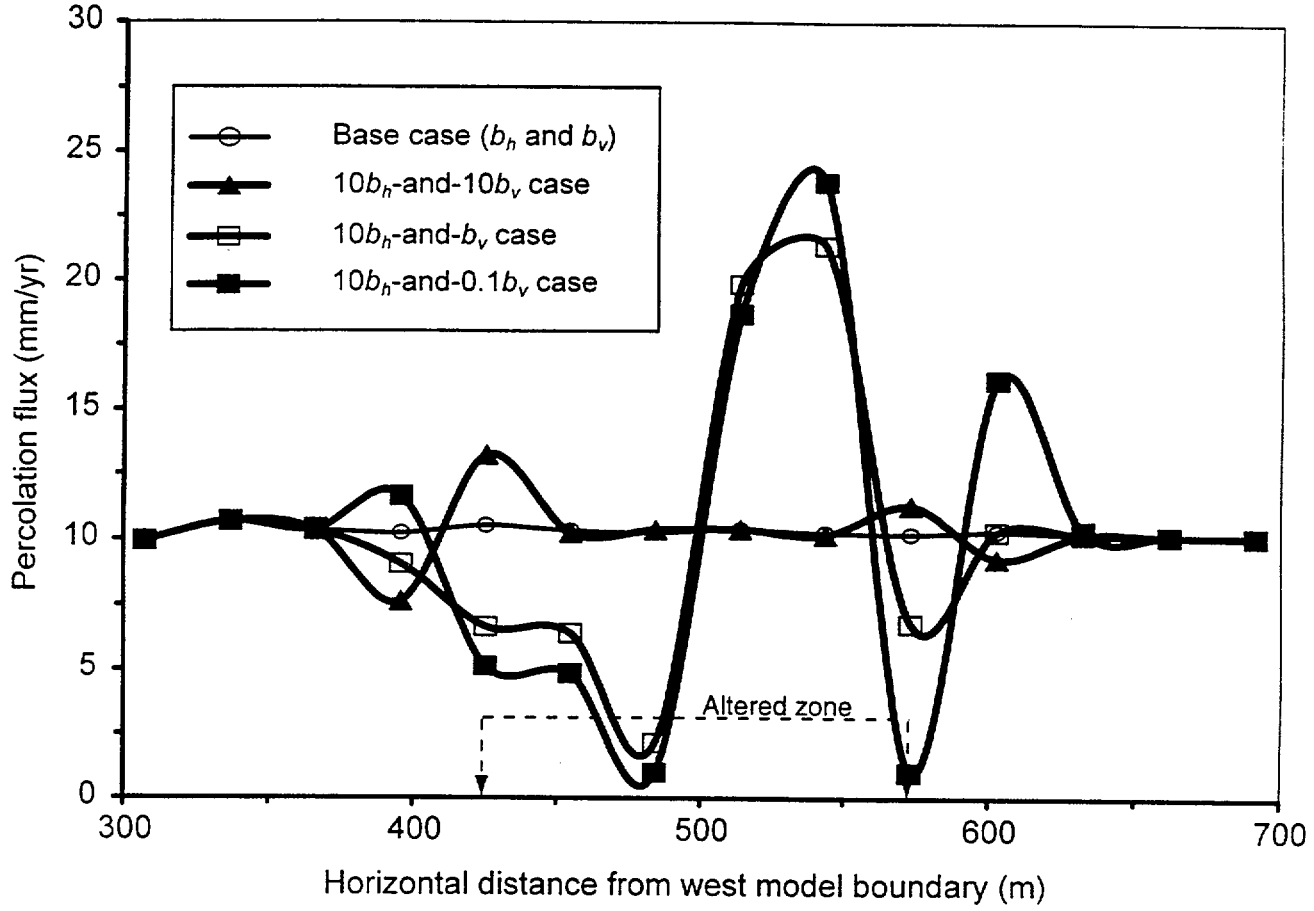

Ofoegbu et al., Fig 9

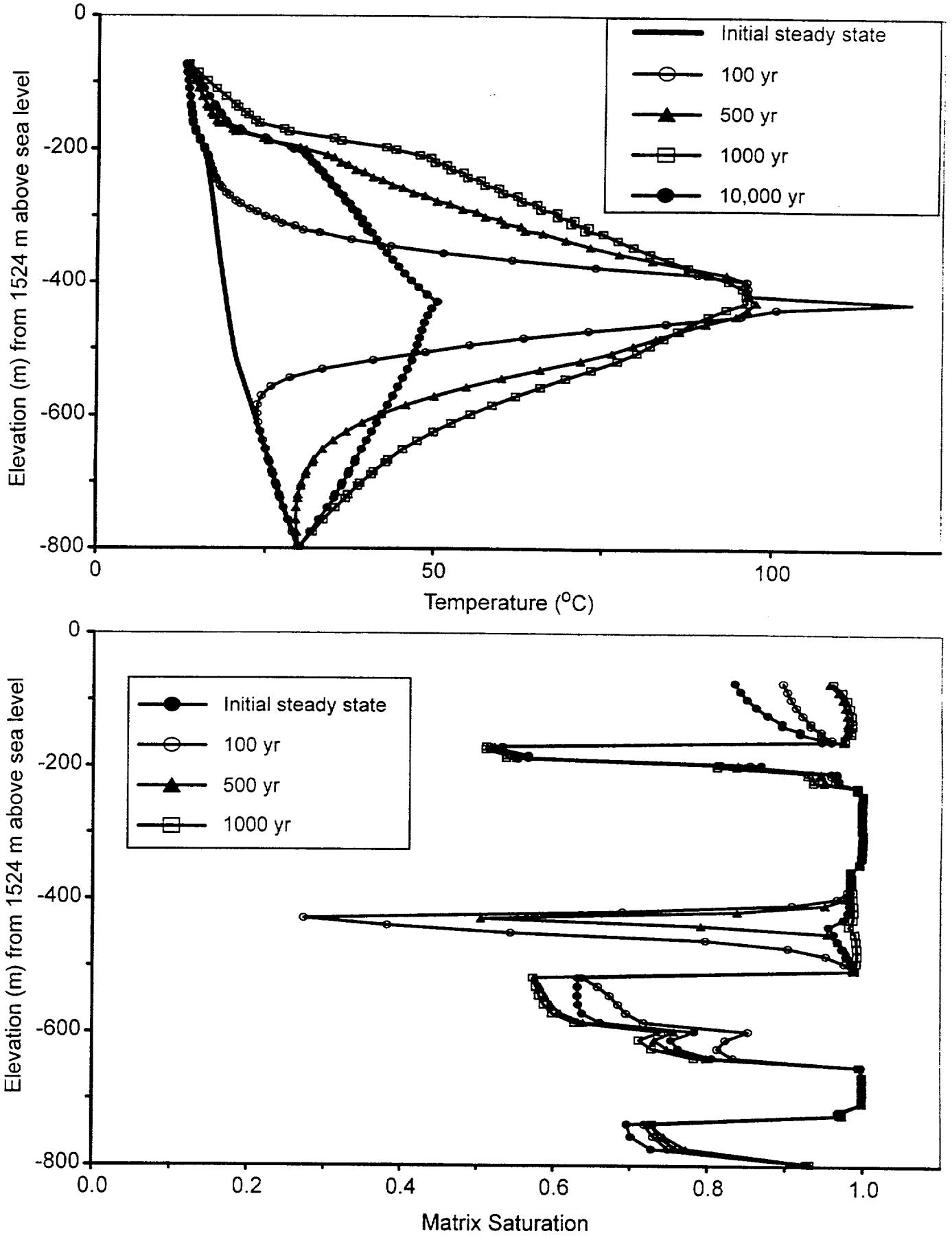

Ofoegbu et al., Fig 10

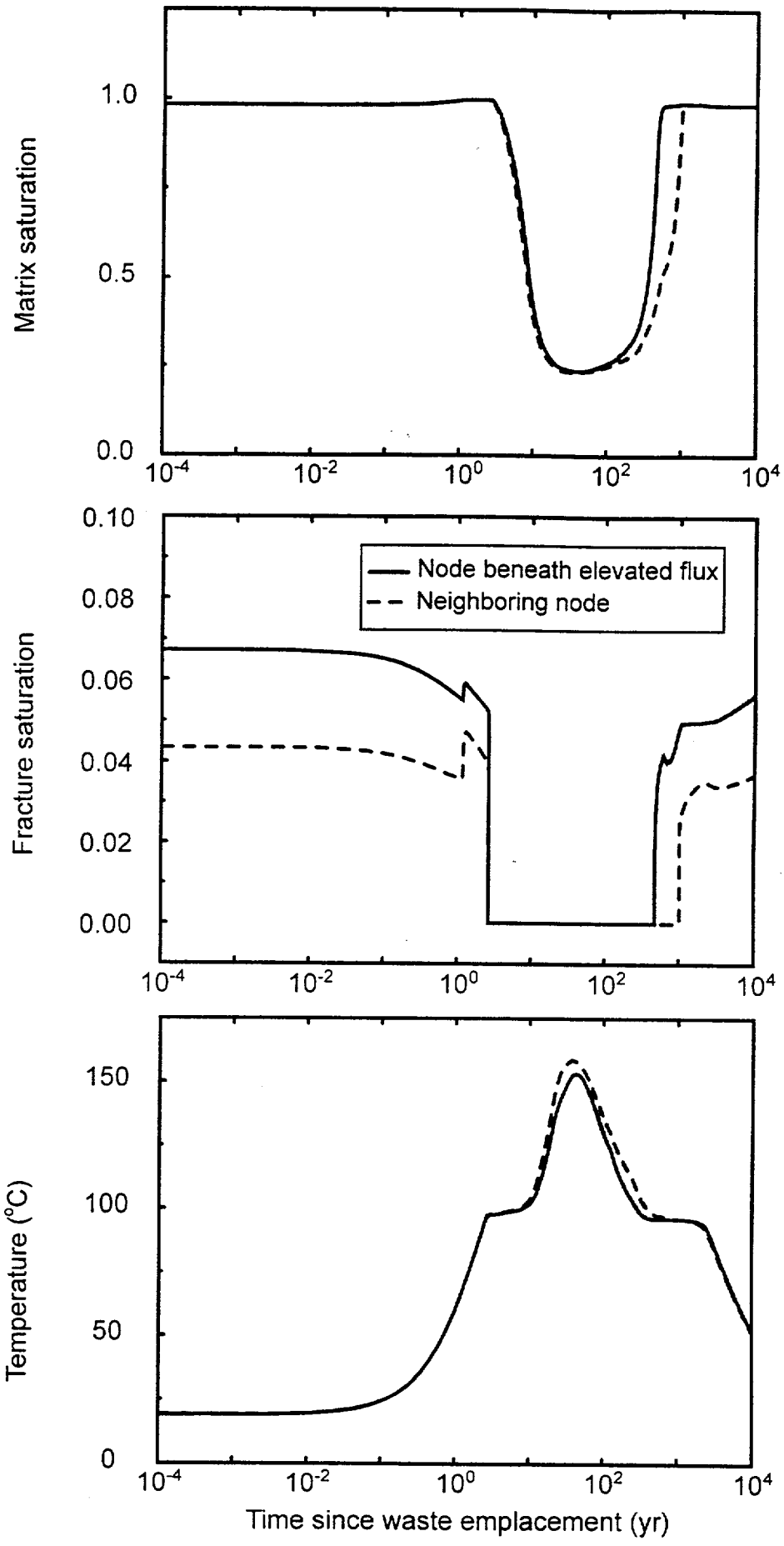

Ofoegbu et al., Fig 11